TÜBİTAK

Turkish Journal of Earth Sciences

http://journals.tubitak.gov.tr/earth/

Research Article

Turkish J Earth Sci
(2016) 25: 103-125

doi:10.3906/yer-1501-35

Geochemistry of Aegean Sea sediments: implications for surface- and bottom-water conditions during sapropel deposition since MIS 5

Ekrem Bursin İŞLER, Ali Engin AKSU*, Richard Nicholas HISCOTT
Department of Earth Sciences, Centre for Earth Resources Research, Memorial University of Newfoundland, St. John's, Newfoundland, Canada

Received: 29.01.2015 • **Accepted/Published Online:** 26.10.2015 • **Final Version:** 08.02.2015

Abstract: Piston cores collected from the Aegean Sea provide a record of sapropel sequence S1, S3–S5. Primary productivity calculations using the equations of Müller and Suess suggest surface paleoproductivities ranged from 180 to 995 g C m^{-2} $year^{-1}$ for sapropels and from 40 to 180 g C m^{-2} $year^{-1}$ for nonsapropel sediments with corresponding total organic carbon values of 9%–12% and 1%–3%, respectively. The higher paleoproductivities exceed those in the most fertile modern upwelling zones, so are probably overestimated. Instead, enhanced preservation, particularly for S4 and S5, likely resulted from poor bottom-water ventilation beneath a salinity-stratified water column. If the preservation factor in the equations of Howell and Thunell is increased to account for such conditions, more realistic paleoproductivity estimates ensue. The interpreted presence of a deep chlorophyll maximum layer for S3–S5 within the lower part of the photic zone may account for high marine organic carbon and increased export production. A deep chlorophyll maximum layer is not advocated for S1 because of the presence of *N. pachyderma* (d) immediately below S1. The organic geochemical data show that both marine and terrestrial organic matter contributed equally to sapropels S3, S4, and S5.

Sapropels S3–S5 were deposited under normal marine conditions with very limited and temporary establishment of near-euxinic bottom-water conditions. Highly depleted and somewhat uniform $\delta^{34}S$ values together with the absence of fully euxinic conditions during sapropel intervals suggest that bacterially mediated sulfate reduction took place consistently below the sediment-water interface. It is believed that climbing levels of primary productivity triggered the onset of sapropel deposition, but that other contemporaneous factors extended and enhanced the conditions necessary for sapropel deposition, including increased nutrient supply from riverine inflow, water column stratification and reduced oxygenation of bottom waters, and buffering of low bottom-water oxygen levels by accumulating terrestrial organic carbon.

Key words: Sapropel S1, S3, S4, S5, paleoceanography, organic geochemistry, Aegean Sea, paleoproductivity

1. Introduction

The composition of the terrigenous fraction in marine sediments reflects the geology of the surrounding landmasses, as well as the predominant sedimentary processes. The terrigenous fraction in the Aegean Sea has sources in the Aegean islands and the drainage basins of moderately sized rivers draining into the Aegean Sea (Figure 1). Several discrete dark-colored sedimentary units rich in organic carbon (referred to as sapropels) have been recognized across the Mediterranean Sea (e.g., Rohling, 1994; Murat and Göt, 2000; van der Meer et al., 2007). These deposits are extraordinary because under normal conditions a large proportion of the organic matter in the ocean is readily oxidized and consumed by bacterial grazing, so does not accumulate on the seafloor. Therefore, sapropel deposition requires substantial modifications within the surface and bottom waters, which are thought to have occurred as a response to distinct changes in the local hydrographic regime and biogeochemical cycling linked to global and regional climatic variations (Rohling et al., 2004 and references therein).

Since the first discovery of Mediterranean sapropels, several hypotheses have been postulated to explain their formation; however, precise mechanisms are still debated. Excess accumulation of organic carbon on the seafloor can occur either due to enhanced preservation following the development of dysoxic to anoxic/euxinic bottom-water conditions (e.g., Demaison and Moore, 1980; Cramp and O'Sullivan, 1999; Emeis et al., 2000; Kotthoff et al., 2008) or when there is increased biological productivity in the surface ocean, which provides higher organic matter fluxes to the seafloor than can be readily oxidized

* Correspondence: aaksu@mun.ca

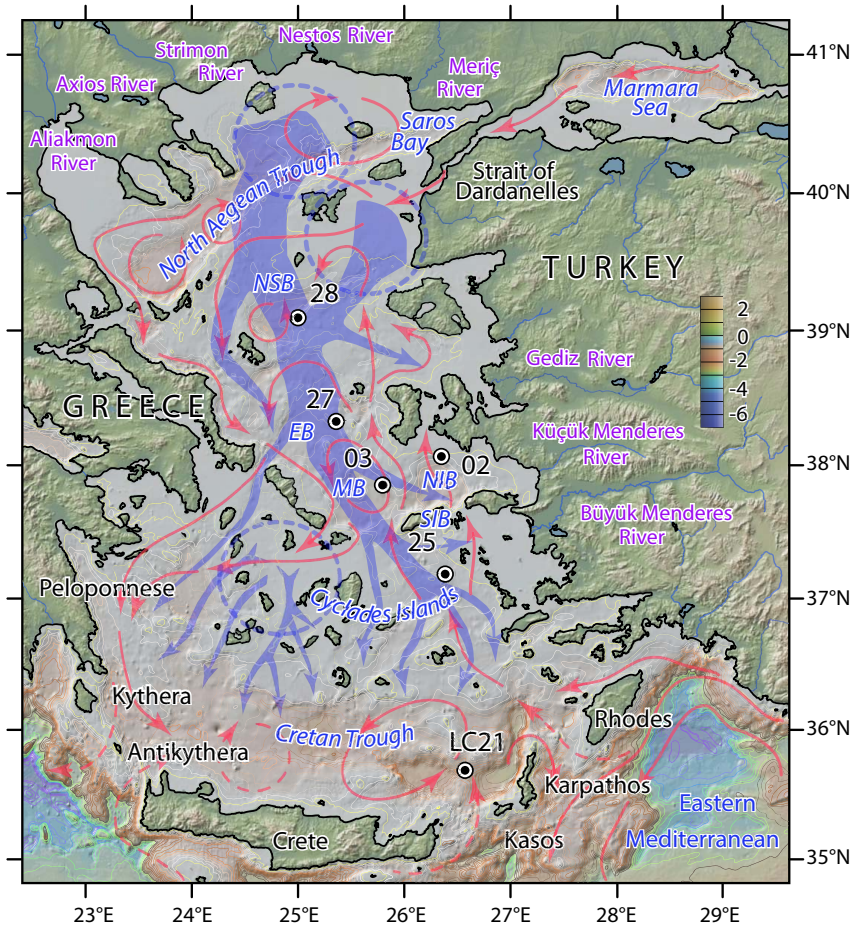

Figure 1. Morphology of the Aegean Sea showing major rivers and the locations of the cores used in this study, and core LC21 (discussed in the text). Bathymetric contours are at 200-m intervals; darker tones in the Aegean Sea indicate greater water depths. NSB = North Skiros Basin, EB = Euboea Basin, MB = Mikonos Basin, NIB = North Ikaria Basin, SIB = South Ikaria Basin. Core names are abbreviated: 02 = MAR03-02, 03 = MAR03-03, 25 = MAR03-25, 27 = MAR03-27, 28 = MAR03-28. Red arrows = surface water circulation from Olson et al. (2006) and Skliris et al. (2010). Elevation scale in kilometers. Bottom-water circulation (blue arrows) from Zervakis et al. (2004) and Gertman et al. (2006). Dashed circles show regions of bottom-water formation.

or bacterially grazed (e.g., Calvert, 1983; Pedersen and Calvert, 1990; van Os et al., 1991; Calvert et al., 1992; Struck et al., 2001; Grelaud et al., 2012). Evidence from previous studies has indicated that sapropel formation is the result of a combination of high organic matter fluxes (ascribed to enhanced export production), intense oxygen consumption in the water column, and reduced oxygen advection to the deeper ocean (Rohling and Gieskes, 1989; Howell and Thunell, 1992; Rohling, 1994; Strohle and Krom, 1997; Casford et al., 2002).

This paper presents multiproxy data from five piston cores of 6–10 m in length from the Aegean Sea and discusses the surface- and bottom-water conditions during times of sapropel formation. It aims to elucidate the primary mechanism(s) leading to increased organic carbon accumulations in the Aegean Sea, and to determine the original environment of high organic carbon accumulation and the roles of preservation of organic matter on the seafloor versus enhanced biological productivity.

1.1. Seabed morphology and hydrography of the Aegean Sea

The Aegean Sea is an elongate embayment that forms the northeastern extension of the eastern Mediterranean Sea (Figure 1). To the northeast, it is connected to the Black Sea through the straits of Dardanelles and Bosphorus and the intervening small land-locked Marmara Sea. In the south, the Aegean Sea communicates with the eastern

Mediterranean Sea through several broad and deep straits located between the Peloponnesus Peninsula, the island of Crete, and southwestern Turkey (Figure 1). The Aegean Sea is divided into three physiographic regions: the northern Aegean Sea, including the North Aegean Trough; the central Aegean plateaus and basins; and the southern Aegean Sea, including the Cretan Trough (Figure 1).

The dominant bathymetric feature in the northern portion of the Aegean Sea is the 800–1200-m-deep depression referred to as the North Aegean Trough (Figure 1). It includes several interconnected depressions and extends in a WSW–SW direction from Saros Bay, widening toward the west. The central Aegean Sea is characterized by a series of relatively shallower (600–1000 m), mainly NE-oriented depressions and their intervening 100–300-m-deep shoals and associated islands (Figure 1). The southern Aegean Sea is separated from the central Aegean Sea by the arcuate Cyclades archipelago, a convex-southward shallow volcanic arc dotted by numerous islands and shoals extending from the southern tip of Euboea Island to southwestern Turkey (Figure 1). A large 1000–2000-m-deep, generally E–W-trending depression, the Cretan Trough, occupies the southernmost portion of the Aegean Sea, immediately north of Crete.

The physical oceanography of the Aegean Sea is controlled primarily by the regional climate, the freshwater discharge from major rivers draining southeastern Europe, and seasonal variations in the Black Sea surface-water outflow through the Strait of Dardanelles (Zervakis et al., 2004). The surface water hydrography is characterized by a large-scale cyclonic circulation, although the most active dynamic features of the Aegean Sea are its mesoscale cyclonic and anticyclonic eddies (Figure 1; Lykousis et al., 2002). A branch of the westward-flowing Asia Minor Current deviates toward the north, out of the eastern Mediterranean basin and into the Aegean Sea, carrying the warm (16–25 °C) and saline (39.2–39.5 psu) Levantine Surface Water and Levantine Intermediate Water along the western coast of Turkey. The Levantine water mass occupies the uppermost 400 m of the water column. The Asia Minor Current reaches the northern Aegean Sea, where it encounters the relatively cool (9–22 °C) and less saline (22–23 psu) Black Sea water and forms a strong thermohaline front. As a result, the water column structure in the northern and central Aegean Sea comprises a surface veneer 20–70 m thick consisting of modified Black Sea water overlying a Levantine intermediate water mass of higher salinity that extends down to 400 m. The water column below 400 m is occupied by the locally formed North Aegean Deep Water with uniform temperature (13–14 °C) and salinity (39.1–39.2 psu; Zervakis et al., 2000, 2004; Velaoras and Lascaratos, 2005). The surface and intermediate waters follow the general counter-clockwise circulation of the Aegean Sea and progressively mix as they flow southwards along the eastern coast of mainland Greece.

Bottom-water formation in the Aegean Sea mainly occurs in two regions in the northern Aegean Sea where there is rapid cooling and downwelling of the Levantine Surface and/or the Black Sea Surface water masses during the winter months (Figure 1; Zervakis et al., 2004; Gertman et al., 2006). Minor deep water formation also occurs in the western portion of the Cyclades. This evolving bottom water mass flows southward, progressively spreading across the deep Aegean Sea basins (Figure 1; Zervakis et al., 2004). Thus, the water column below 400 m in the Aegean Sea is of uniform temperature (13–14 °C) and salinity (39.1–39.2 psu; Zervakis et al., 2000, 2004; Velaoras and Lascaratos, 2005). Previous studies have shown that there is a significant density contrast between the deep waters of the northern-central and southern Aegean basins; in particular, the density values in the north are the highest in the eastern Mediterranean region (29.64 kg m^{-3}; Zervakis et al., 2000). The presence of such high-density bottom waters together with the limited exchange depth (down to ~400 m) suggest that deep water formation in these basins is a local phenomenon that, in turn, leads to the inference that the Aegean Sea, at least north of the Cyclades, behaves as a concentration basin. The rate of deep water formation and the residence time of this water are closely related to the size of each subbasin and the characteristics and circulation of the overlying intermediate layers. Hydrographic surveys show that an influx of Aegean Sea water has replaced 20% of the deep and bottom waters of the eastern Mediterranean Sea, suggesting that the Aegean Sea (in addition to the Adriatic Sea) may play an important role in the physical oceanography of the eastern Mediterranean Sea during highstand conditions like those in effect today (Roether et al., 1996).

2. Materials and methods

Five piston cores and their trigger-weight gravity cores were collected from the Aegean Sea during the 2003 cruise MAR03 of the RV *Koca Piri Reis* of the Institute of Marine Sciences and Technology, Dokuz Eylül University (Figure 1; Table 1). Piston cores were collected using a 9–12-m-long Benthos piston corer (1000-kg head weight) and a 3-m-long trigger-weight gravity corer (300-kg head weight). Core locations were recorded using an onboard Global Positioning System (GPS) receiver. Water depths at the core sites were determined using a 12-kHz echo sounder.

Cores were shipped to Memorial University of Newfoundland where they were split and described. Sediment color was determined using the Rock Color Chart published by the Geological Society of America in 1984.

Table 1. Location and water depth of cores used in this study. A = length of piston core, B = length of gravity core, C = amount of core top loss during coring, D = length of the composite core.

Core	Latitude	Longitude	A (cm)	B (cm)	C (cm)	D (cm)	Water depth (m)
MAR03-02	38°03.97′N	26°22.30′E	776	86	37	813	398
MAR03-03	37°51.72′N	25°49.17′E	580	50	24	604	720
MAR03-25	37°10.36′N	26°26.55′E	604	25	25	629	494
MAR03-27	38°18.68′N	25°18.97′E	952	106	80	1032	651
MAR03-28	39°01.02′N	25°01.48′E	726	165	100	826	453

Cores were systematically sampled at 10-cm intervals for various multiproxy data. At each sampling depth, a 2-cm-wide "half-round" core sample (~20 cm^3) was removed from the working halves of the cores. The outer edge of this sample was scraped to avoid contamination and the sample was then divided into two subsamples: a subsample of ~7 cm^3 for organic geochemical/stable-isotope analyses, and a subsample of ~13 cm^3 for inorganic stable-isotope analyses and planktonic foraminiferal studies.

For oxygen isotopic analyses, the planktonic foraminifera *Globigerinoides ruber* and the benthic foraminifera *Uvigerina mediterranea* were used. For a few samples, where *G. ruber* was absent, *Globigerina bulloides* was picked instead. For planktonic foraminifera, the oxygen and carbon isotopic values of both *G. ruber* and *G. bulloides* are plotted using different colors and scales (see Appendices 1 and 2). There are 30 samples in which both *G. ruber* and *G. bulloides* were analyzed. These samples show a clear and remarkably consistent offset, which can be removed by shifting the oxygen and carbon isotopic curves for *G. bulloides* by ~1‰ (the middle column; Appendices 1 and 2), creating pseudocomposite isotopic curves. These pseudocomposite plots are carried forward into subsequent figures that require the oxygen and carbon isotopic records of cores MAR03-27 and MAR03-28, but with the isotopic values for both *G. ruber* and *G. bulloides* displayed using separate horizontal scales and different colors for clarity.

In each sample, 15–20 *G. ruber* and 4–6 *U. mediterranea* (or 15–20 *G. bulloides*) were hand-picked from the >150-µm fractions, cleaned in distilled water, and dried in an oven at 50 °C. The foraminiferal samples were then placed in 12-mL autoinjector reaction vessels. The reaction vessels were covered with Exetainer screw caps with pierceable septa, and were placed in a heated sample holder held at 70 °C. Using a GC Pal autoinjector, the vials were flushed with ultrahigh-purity He for 5 min using a double-holed needle connected by tubing to the He gas source. Sample vials were then manually injected with 0.1 mL of 100% H_3PO_4 using a syringe and needle. A minimum of 1 h was allowed for carbonate samples to react with the phosphoric acid. The samples were analyzed using a triple collector Thermo Electron Delta V Plus isotope ratio mass spectrometer. Reference gases were prepared from three different standards of known isotopic composition using the same methods employed for the unknown samples, and were used to calibrate each run. The $\delta^{18}O$ and $\delta^{13}C$ values are reported with respect to the Pee Dee Belemnite (PDB) standard.

The amounts of total organic carbon (TOC) and total sedimentary sulfur (TS) and the isotopic composition of TOC and sedimentary sulfur were determined using a CarloErba NA 1500 Elemental Analyzer coupled to a Finnegan MAT 252 isotope-ratio mass spectrometer. Samples were acidified using 30% HCl, and carbonate-free residues were dried overnight in an oven at 40 °C and then powdered. Approximately 15 mg of sample was transferred into 4–6-mm tin capsules, which were then sealed in preparation for analysis. TOC in the samples was converted to CO_2, SO_2, H_2O, and other oxidized gases in the oxidation chamber and then passed through a reduction reagent, a $Mg(ClO_4)_2$ water trap, and a 1.2-m Poropak QS 50/80 chromatographic column at 70 °C for final isolation. The TOC and TS concentrations in the samples were back-calculated as percentages of the dry weight sediment. Isotopic analyses for $\delta^{13}C_{org}$ and $\delta^{34}S$ are reported in standard notation referenced to the standards VPDB and VCDT, respectively.

Stacked planktonic and benthic oxygen-isotope curves were constructed by averaging the age-converted isotopic values of *G. ruber* and *U. mediterranea* in the cores. The 0–110-ka portion of the stacked planktonic oxygen-isotope curve was constructed using the average isotopic values in cores MAR03-2, MAR03-28, and MAR03-27. The section between 110 and 130 ka is based on the $\delta^{18}O$ curve for core MAR03-28. The 0–110-ka portion of the stacked benthic oxygen-isotope curve was constructed using the average isotopic values in cores MAR03-02, MAR03-03, MAR03-25, and MAR03-28. The section between 110 ka and 130 ka is based on the average of the oxygen-isotope values in cores MAR03-3 and MAR03-28. Four samples from cores MAR03-25, MAR03-27, and MAR03-28 were radiocarbon dated (Table 2).

Table 2. Uncalibrated and calibrated AMS ^{14}C ages in foraminiferal samples. Radiocarbon ages are converted into calibrated calendar years (cal yrBP) using the IntCal Marine04 curve with global reservoir correction of 408 years and the program Calib5.0.2 (Stuiver and Reimer, 1993; Hughen et al., 2004a). A local reservoir age correction (ΔR = 149 ± 30 years) was used for the Aegean Sea (Facorellis et al., 1998).

Core	Depth (cm)	Material	^{14}C age (yrBP)	Cal age (yrBP)	Laboratory
MAR03-28P	340	Foraminifera	39,470 ± 1050	42,860 ± 796	BE246398
MAR03-28P	460	Foraminifera	>45,000 ± 1050	47,717 ± 1127	BE246399
MAR03-25P	320	Foraminifera	32,960 ± 280	36,300 ± 325	OXFORD-AX
MAR03-27P	500	Foraminifera	35,910 ± 370	39,933 ± 445	OXFORD-A22427

2.1. Lithostratigraphy

On the basis of macroscopic core descriptions, organic carbon content, and color, four sapropel units and five nonsapropel units are identified and labeled as 'A' through 'I' from top to bottom (Figure 2). The correlation of the units across the five cores was accomplished by matching peaks of oxygen isotopic curves together with the stratigraphic positions of several ash layers (Figure 3; Aksu et al., 2008). Sapropels are distinguished by their comparatively darker colors and their higher TOC contents. However, a quantitative threshold is not considered as a prerequisite for sapropel designation. Instead, a sapropel is recognized

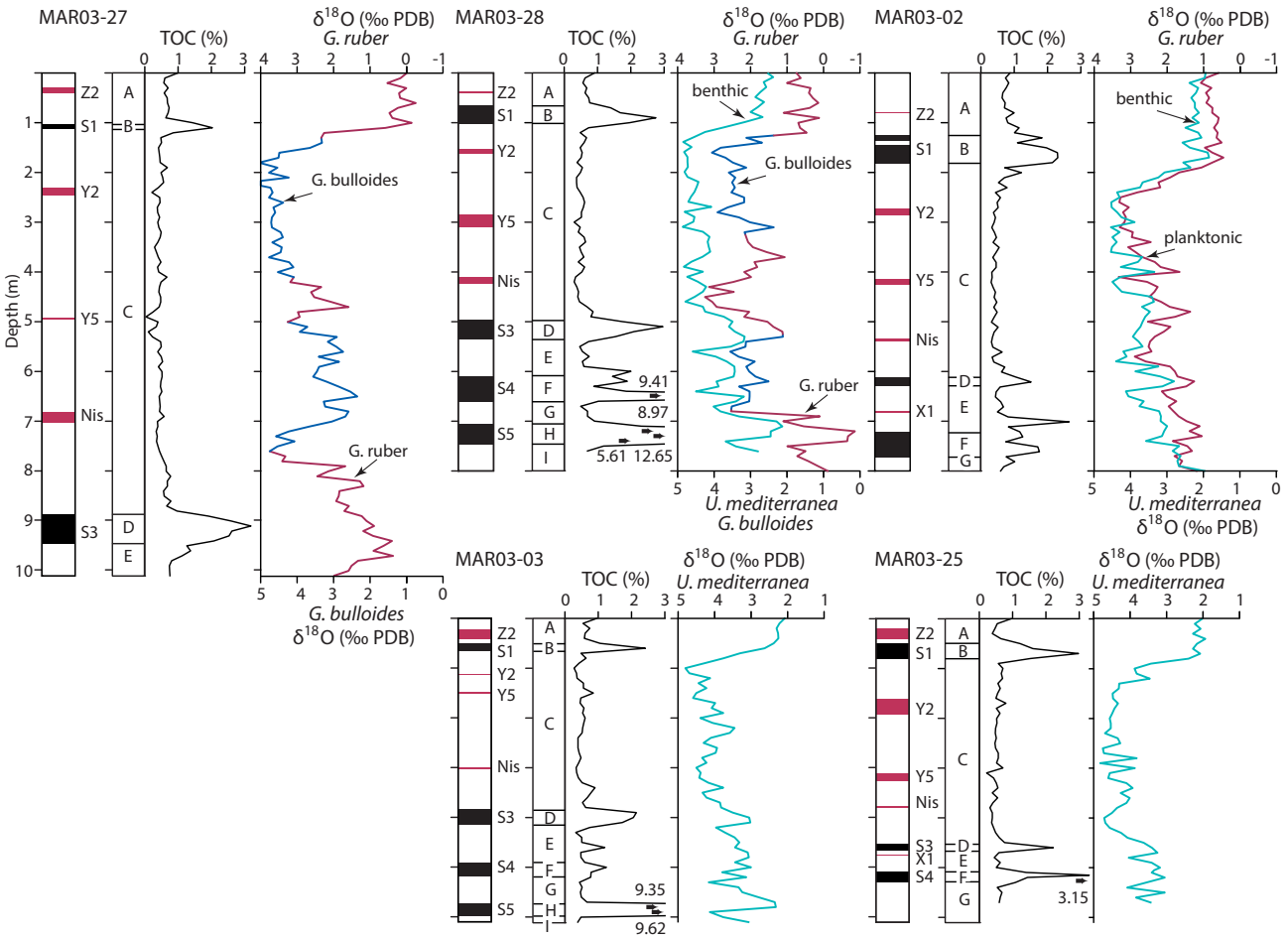

Figure 2. Downcore plots showing the lithostratigraphic units (A through I), total organic carbon (TOC) contents, and variations in oxygen isotope values ($\delta^{18}O$) in the Aegean Sea cores. Red and blue lines are the $\delta^{18}O$ values in planktonic foraminifera *G. ruber* and *G. bulloides*, respectively; aquamarine lines are the $\delta^{18}O$ values in benthic foraminifera *U. mediterranea*. MIS = marine isotopic stages. Black fills = sapropels, red fills = volcanic ash layers (from Aksu et al., 2008). Core locations are shown in Figure 1.

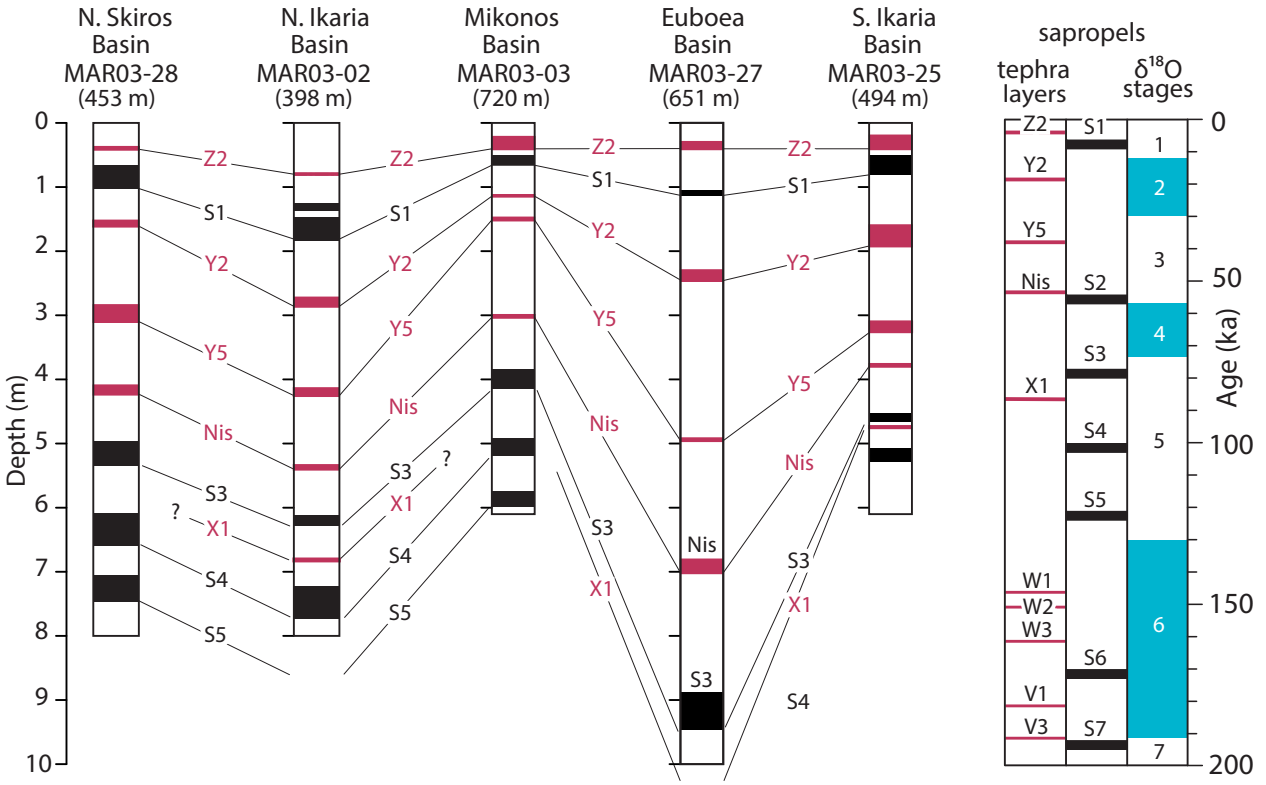

Figure 3. Correlation of ash layers (red) and lithostratigraphic units across the Aegean Sea cores. Ash layers Z2, Y2, Y5, Nis, and X1 (red fills) are from Aksu et al. (2008). Sapropels are shown as black fills with S1, S3, S4, and S5 designations. Global oxygen isotopic stage boundaries are from Lisiecki and Raymo (2005). Core locations are shown in Figure 1. Numbers in brackets below core identifiers are water depths.

when the organic carbon content is twice the background level measured in underlying and overlying units (Figure 2). Macroscopically, both sapropel and nonsapropel sediments are composed of slightly to moderately burrowed sand-bearing muds and silty muds (Figure 4). Lack of evidence for resedimentation (e.g., graded beds, sand/silt to mud couplets), paucity of terrigenous sand-sized material, and ubiquitous presence of bioturbational mottling throughout the cores collectively suggest that the sedimentation was predominantly through hemipelagic rain. The sand fraction is predominantly composed of volcanic tephra as well as biogenic remains including foraminifera, pteropods, and bivalve and gastropod shells.

Nonsapropel units A, C, E, G, and I are composed of burrow-mottled foraminifera-bearing calcareous clayey muds (Figure 4). These units are predominantly yellowish/dark yellowish brown (10YR5/4, 10YR4/2) and gray (yellowish, light and dark; 5Y5/2, 5Y6/1, 5GY6/1 gray) (Figure 4). The average TOC content is 0.5% and mainly ranges between 0.4% and 0.7% with relatively higher organic carbon contents in unit G, reaching 0.9% (Figure 2). Unit A contains an ash layer that is largely disseminated in fine mud. The ash is widespread throughout the Aegean Sea and part of the eastern Mediterranean Sea and has been identified as the Z2 tephra from the Minoan eruption of Santorini Island (Aksu et al., 2008).

Unit C contains three tephra layers that were described and identified by Aksu et al. (2008): (i) the Y2 tephra associated with the Cape Riva eruption on the island of Santorini (also known as the Akrotiri eruption), (ii) the Y5 tephra related to the Campanian Ignimbrite eruption of the Phlegraean Fields of the Italian Volcanic Province, and (iii) the Nisyros tephra associated with the Nisyros eruptions on the island of Nisyros. These ash layers form discrete beds with discernible sharp bases and tops in the cores, with thicknesses ranging from 3 to 53 cm (Figure 4). Unit E contains an ash layer disseminated in mud in cores MAR03-25 and MAR03-2. This tephra layer is correlated with the X1 tephra, most likely derived from the Aeolian Islands, Italy (Aksu et al., 2008).

Sapropel units B, D, F, and H are distinguished from overlying/underlying units by their darker olive gray color (5Y4/1, 5Y3/2, 5Y4/2, 5Y5/2, 5Y2/2, 5Y2/1). They are composed of color-banded clayey mud with a sharp base, overprinted by sharp-walled and oval-shaped burrows ~1 mm in diameter identified as *Chondrites* (Figure 4). The

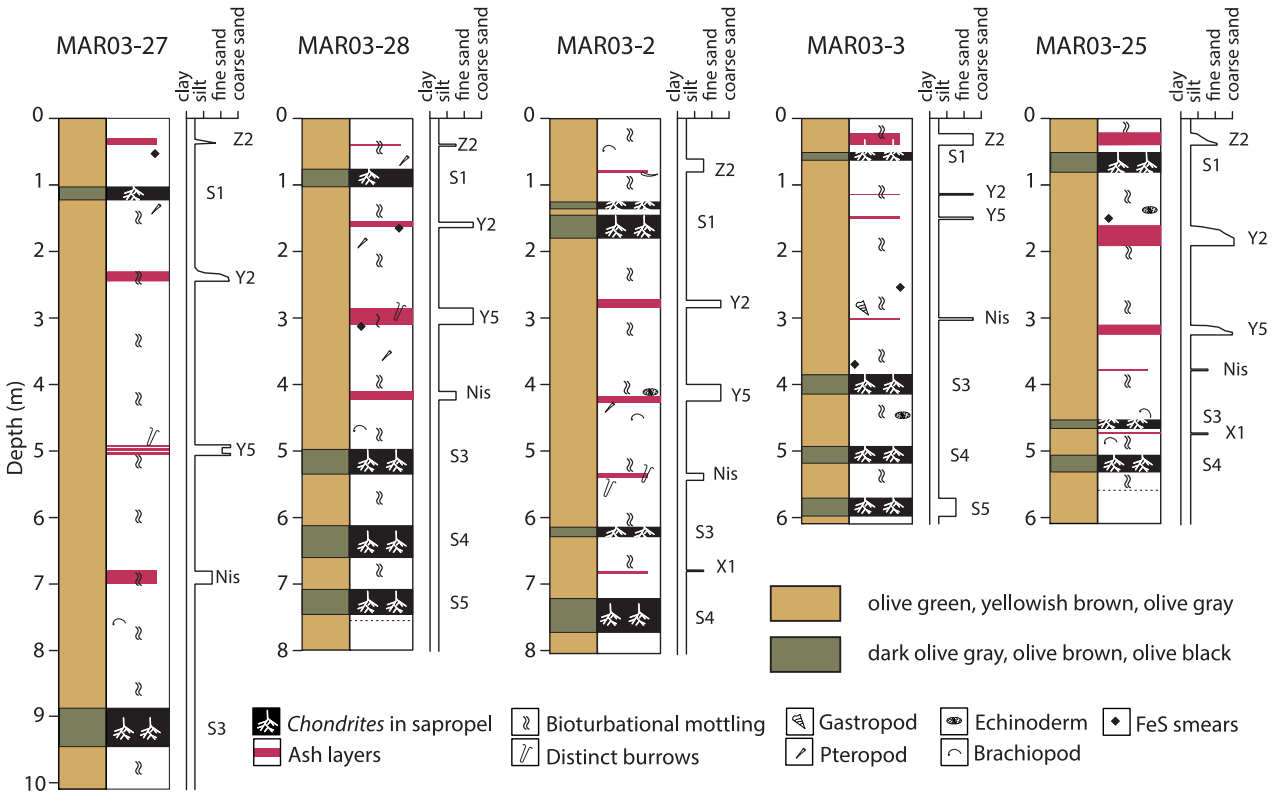

Figure 4. Lithological units in the Aegean Sea cores. Details of the core colors are given in the text. Core locations are shown in Figure 1.

organic carbon contents display significant variations among sapropel units ranging between 1% and 12.65% (Figure 2).

2.2. Age models

The cores were converted from a depth domain to a time domain using a number of age control points (Figure 5; Table 3). The control points include (i) beds/units for which the ages are well constrained, including the most recent sapropel layer S1 and the tephra layers Z2, Y2, and Y5, and (ii) points determined by curve matching of the oxygen-isotope signals from the cores with those in the global oxygen-isotope curve of Lisiecki and Raymo (2005). Maximum isotopic enrichments are considered more reliable than depleted values for the purposes of curve matching because the depleted oxygen-isotope signals, particularly high amplitude values, can be generated by local/episodic changes (e.g., river input pulses) and, accordingly, might not correspond to global climatic changes.

The tephra ages used in this paper come from dating of the associated eruptions on land (summarized in Aksu et al., 2008) because these are more direct measurements than ages interpreted from marine cores (e.g., Satow et al., 2015). Recent refinements to the age model for the $\delta^{18}O$ record of the eastern Mediterranean area (Grant et al., 2012) are consistent with the global curve of Lisiecki and Raymo (2005) at the level of resolution of the cores considered in this paper. This is demonstrated by the excellent correspondence of all prominent peaks and troughs of the Lisiecki and Raymo (2005) curve with the isotopic curve from U/Th-dated speleothems of Soreq cave, Israel (Figure 5; Soreq cave data from Grant et al., 2012, their supplementary data, worksheet 2, columns I and J). In particular, the age picks of the control points used in this paper differ by no more than 1 ka from where equivalent points are found on the Soreq cave plot.

The depth-to-age conversion reveals that the oldest sediment recovered in the cores (unit I) dates from ~130 ka at the transition from MIS 6 to MIS 5 (Figure 5). The interpolated basal ages of sapropels S3, S4, and S5 are 83.2–80.4 ka, 106.4–105.8 ka, and 128.6–128.4 ka, respectively (Table 4). These ages are in good agreement with the previously published ages of sapropels S3, S4, and S5 during MIS 5a, 5c, and 5e in the eastern Mediterranean Sea (Figure 5; Rossignol-Strick, 1985; Emeis et al., 2003).

3. Results

3.1. Oxygen isotopes

The age-converted stacked $\delta^{18}O$ curves for planktonic and benthic foraminifera illustrate that there are predictable

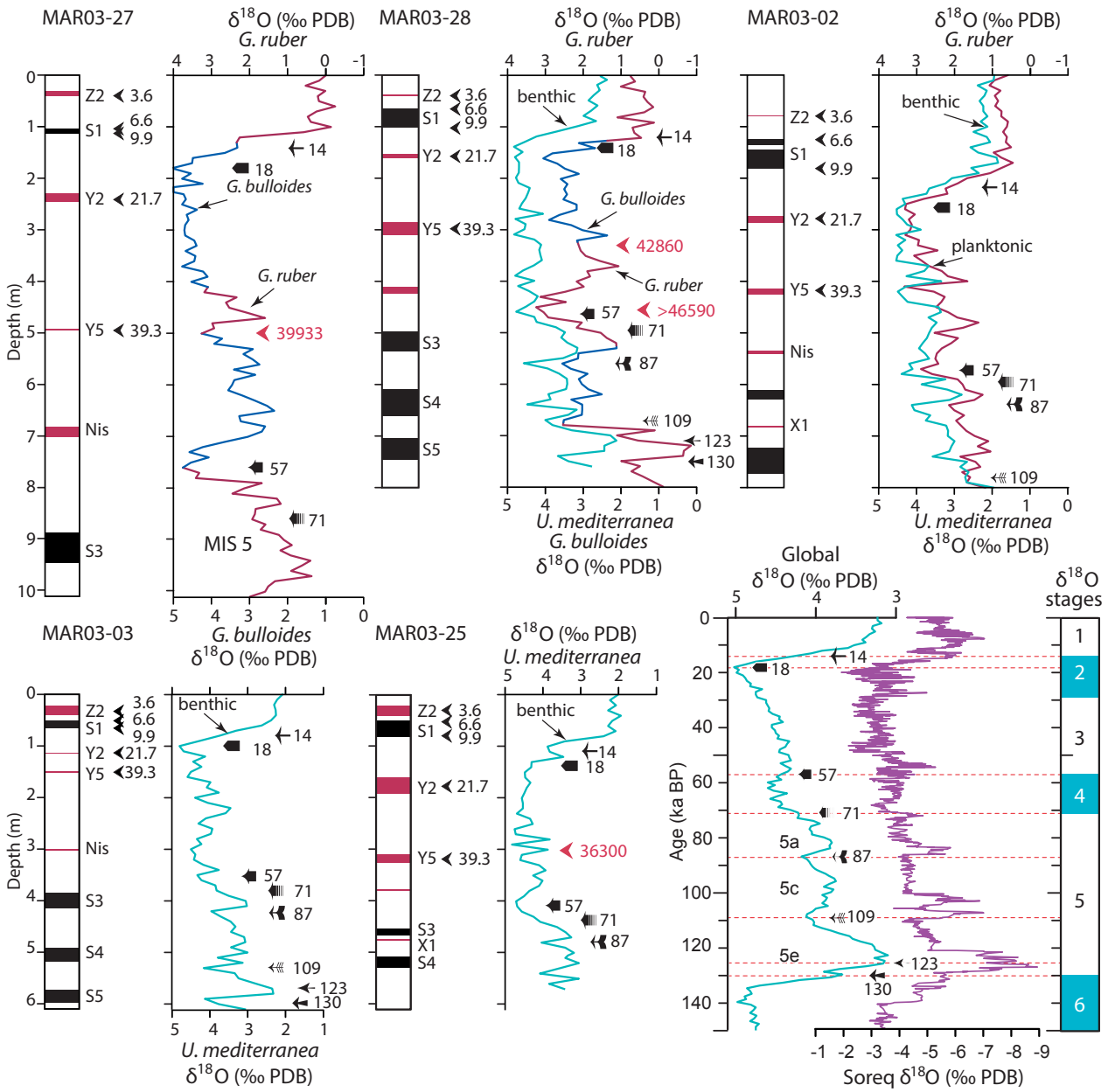

Figure 5. Age control points (in 1000 years) used for the depth-to-age conversion of the multiproxy data in the Aegean Sea cores (see Table 3). Triangular arrows are those obtained from the known ages of top/base S1 and the tephra layers Z2, Y2, and Y5. Other arrows symbolize age control points determined by matching of the oxygen isotope curves with the global curve of Lisiecki and Raymo (2005), consistent in its chronology with the speleothem-based $\delta^{18}O$ record from Soreq cave, Israel (Grant et al., 2012). Red and blue lines are the $\delta^{18}O$ values in planktonic foraminifera *G. ruber* and *G. bulloides*, respectively; aquamarine lines are the $\delta^{18}O$ values in benthic foraminifera *U. mediterranea*. Red fills = volcanic ash layers (from Aksu et al., 2008). Red numbers with arrows are calibrated radiocarbon ages (see Table 2). Core locations are shown in Figure 1.

variations in oxygen isotopic composition of the Aegean Sea during the last 130 ka. Moderate to large amplitude excursions in the $\delta^{18}O$ records correspond to glacial and interglacial stages (Figure 6). For example, the ~4‰ $\delta^{18}O$ depletions in the upper segments of the cores mark the MIS 2–1 transition (Figure 6). The prolonged enrichment of ~3‰ in planktonic foraminiferal $\delta^{18}O$ values in the middle portions of the cores (80–60 ka) reflects the transition from MIS 5 to MIS 4 (Figure 6). The abrupt enrichment of ~3‰ within MIS 5 is associated with the transition from MIS 5e to 5d. MISs 1, 3, 5a, 5c, and 5e are marked by moderately depleted (~1.2‰ in MIS 3) to highly

Table 3. Control points used in the construction of the chronology in the Aegean Sea cores. The ages of the marine isotope stages (MIS) are from Lisiecki and Raymo (2005), the ages of the tephra layers are from Aksu et al. (2008), the ages of sapropel S1 are from İşler et al. 2015), and ^{14}C dates are from Table 2.

		MAR03-28	MAR03-02	MAR03-03	MAR03-25	MAR03-27
Control points	Age (years)	Depth (cm)	Depth (cm)	Depth (cm)	Depth (cm)	Depth (cm)
Z2 tephra	3613	40	80	33	20	40
S1top	6600	65	125	51	50	104
S1base	9900	102	181	66	81	113
MIS1/2	14,000	120	220	80	110,5	142
MIS2 max	18,000	141	259	100	138	180
Y2 tephra	21,554	161	286	113	190	245
^{14}C date	36,300	-----	-----	-----	320	-----
^{14}C date	39,933	-----	-----	-----	-----	500
Y5 tephra	39,280	310	425	151	324	495
^{14}C date	42,860	340	-----	-----	-----	-----
MIS 3/4	57,000	460	574	353	410	760
MIS 4/5	71,000	496	597	381	438	860
MIS 5.2	87,000	560	640	425	480	-----
MIS 5.4	109,000	672	783	531	-----	-----
MIS 5.5	123,000	710	-----	571	-----	-----
MIS 5/6	130,000	750	-----	600	-----	-----

Table 4. Calculated ages of sapropels S3, S4, and S5 in the Aegean Sea cores compared to those identified in core LC21 from the Cretan Trough (Grant et al., 2012).

Cores		S3	S4	S5
MAR03-02	Onset	82,800	106,400	-------
	End	76,600	94,400	-------
MAR03-03	Onset	83,200	105,800	128,600
	End	72,600	100,600	123,600
MAR03-25	Onset	81,600	105,600	-------
	End	76,800	97,800	-------
MAR03-27	Onset	80,400	-------	-------
	End	74,000	-------	-------
MAR03-28	Onset	80,600	105,800	128,400
	End	70,800	96,200	121,000
LC21	Onset	86,140	108,600	128,390
	End	82,950	100,950	121,280

depleted planktonic foraminiferal δ^{18}O (0.2‰–0.6‰ in MIS 1 and MIS 5), suggesting warmer and possibly less saline conditions. Planktonic foraminiferal δ^{18}O values are notably heavier during MIS 2 and 4 (~2.8‰–3.2‰ in MIS 2 and MIS 4), suggesting cooler and possibly more saline conditions (Figure 6). These δ^{18}O oscillations can be readily correlated with the global oxygen isotopic data (Figure 6; Lisiecki and Raymo, 2005). The depleted δ^{18}O values during MIS 1 and MIS 5 show clear association with times of sapropel deposition. The data show that

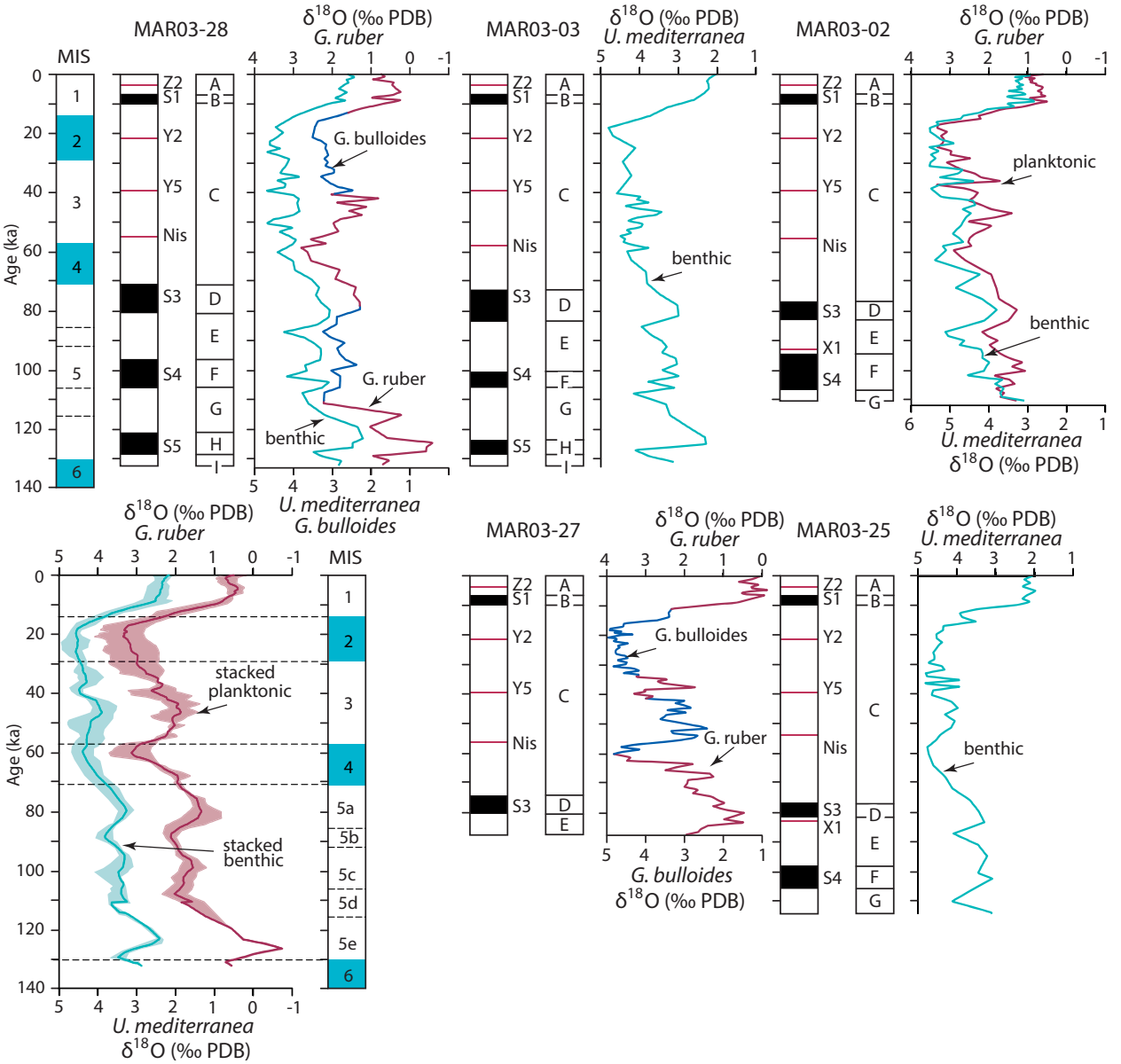

Figure 6. Downcore plots showing the age of the lithostratigraphic units (A through I), total organic carbon (TOC) contents, and the variations in oxygen isotope values ($\delta^{18}O$) in the Aegean Sea cores. Red and blue lines are the $\delta^{18}O$ values in planktonic foraminifera *G. ruber* and *G. bulloides*, respectively; aquamarine lines are the $\delta^{18}O$ values in benthic foraminifera *U. mediterranea*. MIS = marine isotopic stages. Black fills = sapropels, red fills = volcanic ash layers (from Aksu et al., 2008). Core locations are shown in Figure 1.

depletions are strongest during and immediately following the accumulation of sapropels S1 and S5, ranging from 0.6‰ to 0.9‰ in *U. mediterranea* and from 0.3‰ to 0.6‰ in *G. ruber* (Figure 6). In sapropels S3 and S4, $\delta^{18}O$ values show similar yet modest variations changing on average between 1.4‰ and 1.8‰ relative to adjacent units. In cores MAR03-28 and MAR03-02, the planktonic and benthic $\delta^{18}O$ values demonstrate similar magnitude depletions and enrichments (Figure 6). Such close covariation allows credible interpretations of the surface-water conditions for cores for which only benthic foraminiferal $\delta^{18}O$ data are available.

3.2. Elemental carbon and sulfur (TOC, TS)

The TOC and TS percentages show close covariation in the Aegean Sea cores. Across nonsapropel intervals, the TOC and TS values fluctuate between 0.3% and 0.6% and between 0.1% and 0.4%, respectively (Figures 7 and 8). In cores MAR03-27, MAR03-25, and MAR03-28, sulfur concentrations are higher between 40 and 18

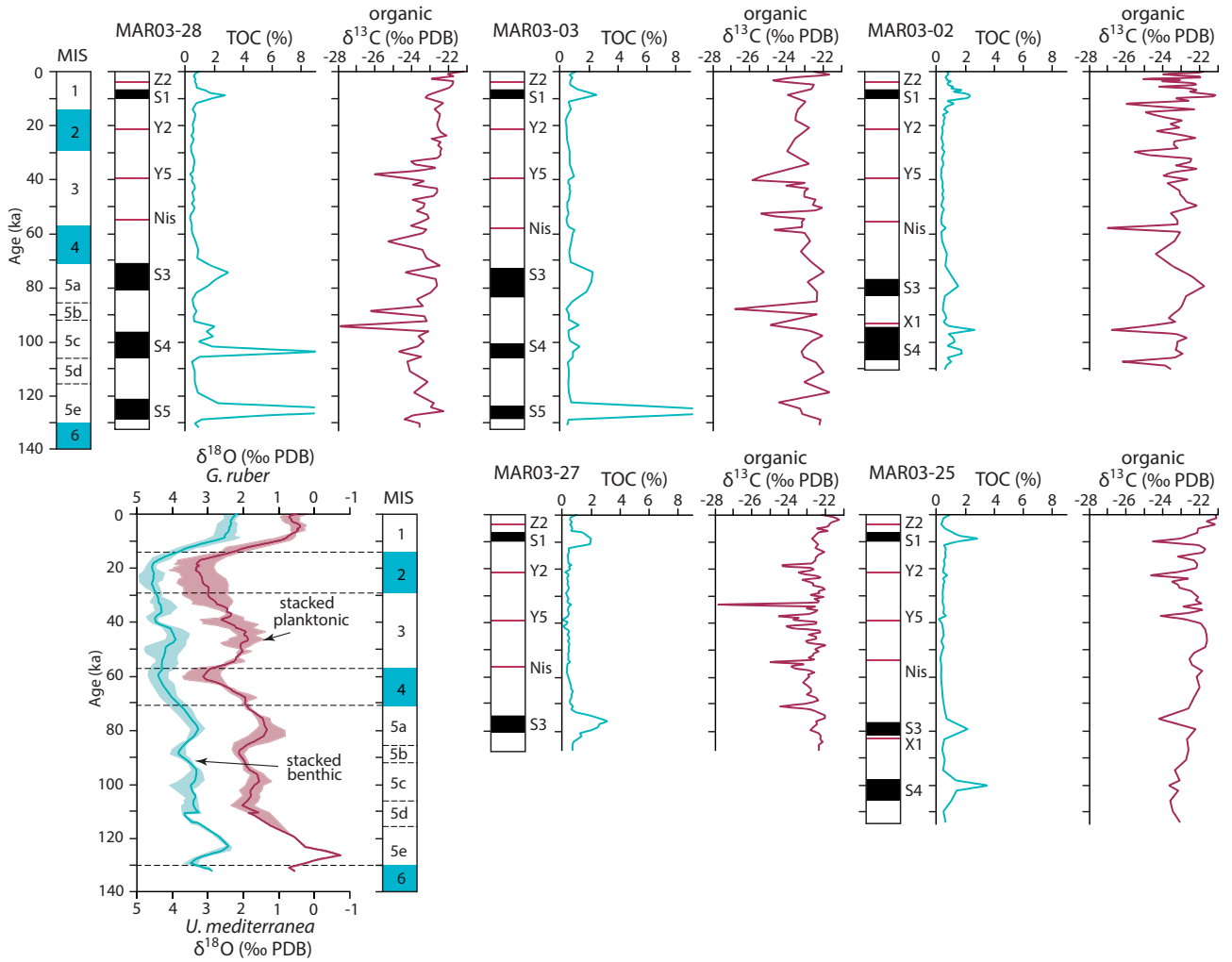

Figure 7. Downcore plots showing the total organic carbon (TOC) contents and the variations in organic carbon isotopic composition ($\delta^{13}C$) in the Aegean Sea cores. MIS = marine isotopic stages. Black fills = sapropels, red fills = volcanic ash layers (from Aksu et al., 2008). Stacked oxygen isotope curves are from Figure 6. Core locations are shown in Figure 1.

ka, showing values ranging generally from 0.4% to 1% (cores MAR03-28 and MAR03-3; Figure 8). Within the most recent sapropel S1, organic carbon content varies from 1.1% in core MAR03-2 to 2.98% in core MAR03-25 (Figure 7). In core MAR03-2, it changes upward from 2.3% to 1.1% to 1.8%, suggesting two peaks of organic matter accumulation in the North Ikaria Basin. The intervening decline in organic-matter accumulation is not recognized in the other cores, either because it is not present or because it was not captured by the 10-cm sample spacing. In sapropel S3, the TOC content ranges from 1.05% to 2.97%, averaging 1.74%. In sapropel S4, maximum and minimum TOC contents of 9.41% and 0.47% are observed in cores MAR03-28 and MAR03-3; it is certainly a nonsapropel mud in the latter core (Figure 7). Moreover, in cores MAR03-2, MAR03-3, and MAR03-28, organic carbon percentages display fluctuations across S4 creating a double-peaked plot, becoming lower in TOC contents within the mid-portions ranging from 0.47% to 0.83%. Sapropel S5 contains the highest organic carbon content, reaching 12.65% at its middle in core MAR03-28, and shows a noticeably higher average TOC content than the upper sapropels, with values of 9.49% and 6.15% in cores MAR03-28 and MAR03-3, respectively (Figure 7).

TS values range from 0.5% to 1.6% in sapropel S1. In parallel to the S3 TOC concentrations, higher TS abundances are observed in sapropel S3 in cores MAR03-28 and MAR03-27, reaching 1.2% and 2.4%, respectively (Figure 8). In sapropel S4, TS values range from 0.8% to 1.35%. In core MAR03-28, both the TOC and TS concentrations show a prominent spike within the lower portions of S4 where they increase to 9.65% and 3.5%. Maximum TS values are 2.8% in sapropel S5 (Figure 8).

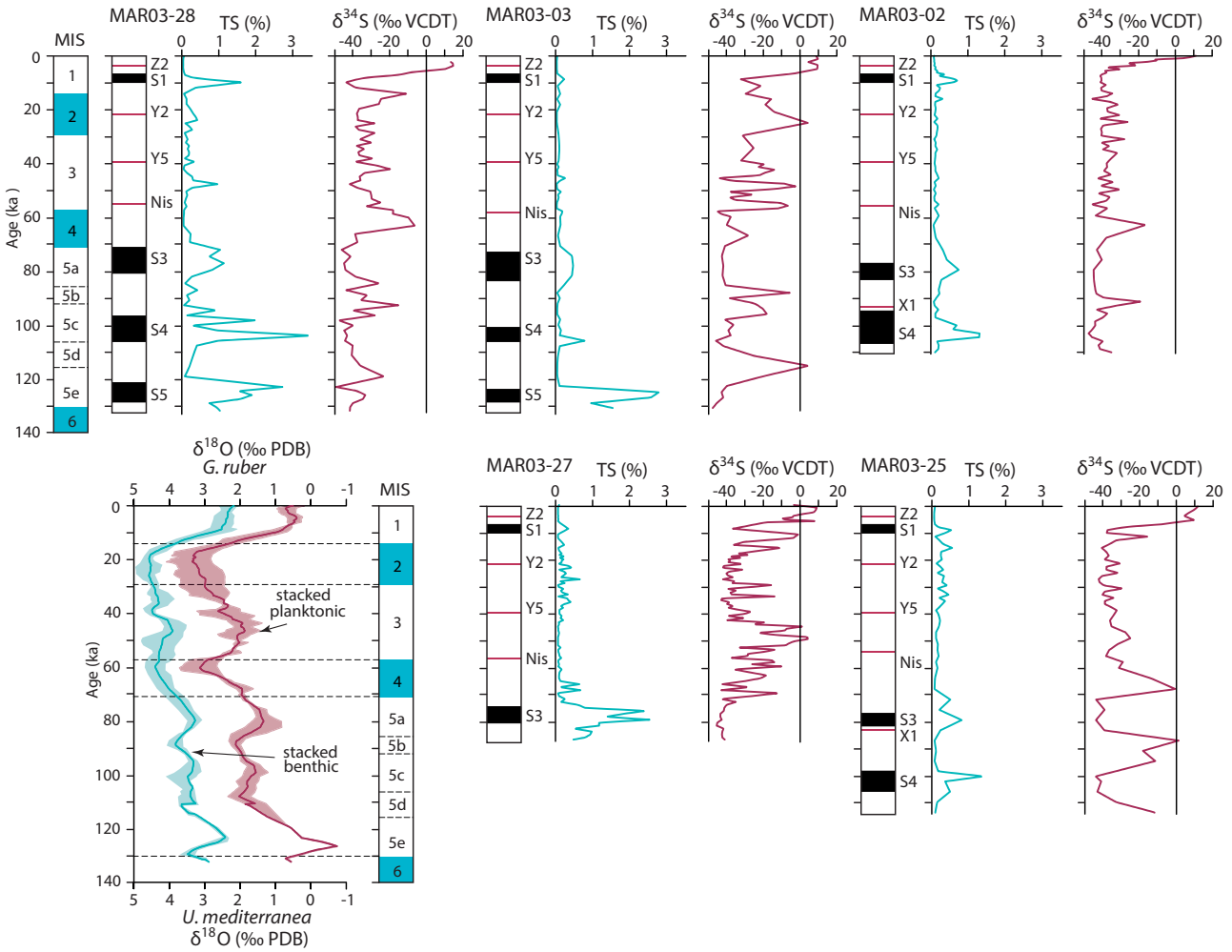

Figure 8. Downcore plots showing the total sedimentary sulfur (TS) contents and the variations in the sedimentary sulfur isotopic composition ($\delta^{34}S$) in the Aegean Sea cores. MIS = marine isotopic stages. Black fills = sapropels, red fills = volcanic ash layers (from Aksu et al., 2008). VCDT = Vienna Canyon Diablo Troilite. Stacked oxygen isotope curves are from Figure 6. Core locations are shown in Figure 1.

3.3. Carbon and sulfur isotopes ($\delta^{13}C_{org}$ and $\delta^{34}S$)

The $\delta^{13}C_{org}$ values range between –22.5‰ and –24‰ with episodic intervals showing maximum depletions of about –27‰ (Figure 7). Sapropels S3, S4, and S5 are characterized by slight enrichments in $\delta^{13}C_{org}$ values with respect to the intervening nonsapropel sediments. This is not the case for S1, which does not show a consistent pattern of $\delta^{13}C_{org}$ variation from one core to another.

Sulfur isotopes show large fractionations of 40‰–50‰ within the uppermost portions of the cores and across MIS 5 associated with interstadial/stadial transitions (Figure 8). Maximum depletions are observed within sapropels S3, S4, and S5 where $\delta^{34}S$ values range between –38‰ and –45‰. Cores MAR03-28, MAR03-25, MAR03-27, and MAR03-2 exhibit similar upward trends between sapropel S3 and S1. A high amplitude positive excursion changing by as much as 42‰ in core MAR03-25, above sapropel S3, is followed by consistently more depleted small amplitude changes until below the most recent sapropel S1 (around 17–20 ka), where an abrupt enrichment occurs prior to sapropel S1 onset (except in core MAR03-2). A persistent enrichment in $\delta^{34}S$ starts at the onset or middle portions of sapropel S1 and continues until the core tops with shifts of as much as 52‰ (core MAR03-28; Figure 8).

3.4. Benthic foraminifera

In this study, benthic foraminiferal assemblages are not described in detail; however, benthic foraminifera were examined in samples from sapropels S3, S4, and S5. These samples contain a low-abundance and low-diversity benthic foraminiferal fauna dominated by *Globobulimina affinis*, *G. pseudospinescens*, *Chilostomella mediterranensis*,

Bolovina alata, *B. attica*, *Bulimina clara*, and *Uvigerina peregrina curticosta*. This benthic foraminiferal faunal assemblage indicates nutrient-rich, oxygen-poor bottom waters during the deposition of MIS 5 sapropels S3, S4, and S5. *G. affinis*, *G. pseudospinescens*, and *C. mediterranensis* cooccurring with *Bolivina* species are also reported in several sapropels from the eastern Mediterranean Sea (Cita and Podenzani, 1980; Herman, 1981; Mullineaux and Lohmann, 1981; Stefanelli et al., 2005; Abu-Zied et al., 2008; Melki et al., 2010) and are known to be abundant in oxygen-poor (dysoxic) bottom water conditions (Ross and Kennett, 1984; McCorkle et al., 1990; Stefanelli et al., 2005; Abu-Zied et al., 2008; Melki et al., 2010).

4. Discussion

4.1. Bottom-water conditions

Sedimentation rates, bottom-water conditions (i.e. oxic, suboxic, dysoxic, anoxic/euxinic), the amount of export production, and bioturbation are the primary factors controlling the deposition of organic carbon in the oceans. The role of dissolved oxygen in the preservation of organic matter in marine sediments has been a subject of considerable debate. High concentrations of organic carbon in marine sediments might be attributed to deposition beneath an O_2-free (euxinic) water column (Demaison and Moore, 1980) where anaerobic processes of organic carbon decomposition are less efficient than decomposition in the presence of dissolved oxygen. However, sedimentation rate plays a significant role as shown by the fact that at high rates (i.e. >40 cm ka^{-1}) preservation of organic carbon does not vary with the dissolved oxygen content of the bottom waters and decomposition occurs mostly under anaerobic conditions below the sediment–water interface. At sedimentation rates of <40 cm ka^{-1}, enhanced preservation requires bottom waters with low dissolved oxygen content or euxinic environments. Because sedimentation rates are calculated to be always <40 cm ka^{-1} throughout the eastern Mediterranean Sea including the Aegean Sea, the enhanced accumulation of organic carbon leading to sapropel formation must be explained by some combination of low bottom-water oxygen contents and enhanced rates of export production.

4.1.1. Source of organic matter

In sapropels, $\delta^{13}C_{org}$ values cluster within narrow ranges, varying from –23.7‰ to –23‰ in sapropel S4, –23‰ to –22‰ in sapropel S3, and –23.2‰ to –22.2‰ in sapropel S5 (Figure 9). These small variations indicate a spatial uniformity of the organic carbon isotopic values during sapropel formation with a slightly higher terrigenous component in S4. Unlike older sapropels, S1 demonstrates larger variations in $\delta^{13}C_{org}$ values (–21.1‰ to –24.7‰), suggesting stronger fluctuations between marine and terrestrial organic-matter input (Figure 9). Significant increases in riverine and Black Sea water input might account for these fluctuations.

Organic carbon isotopic values have been used to identify the sources of organic matter using a linear mixing model (e.g., Fontugne and Calvert, 1992; Aksu et al., 1995a). Although the end members for the marine and terrestrial components have been reported to be –22‰ and –27‰ (Deines, 1980), it is difficult to accurately determine the end members. Considering the range of measured $\delta^{13}C_{org}$ values (between –21.5‰ and –27.4‰) and those from the eastern Mediterranean Sea (maximum of –19.5‰), it is reasonable to assume a range of –18‰ to –20‰ for the marine end member and –28‰ for the terrestrial end member. Therefore, values of –19‰ and –28‰ are used as the marine and terrestrial end members, respectively. Calculations using a linear mixing model show that terrestrial- and marine-sourced organic carbon contributed nearly equally during the deposition of sapropels S5, S4, and S3 (Figure 9). In sapropel S1, the $\delta^{13}C_{org}$ values are lighter at the bottom but become heavier towards the top, implying that fluvial delivery of isotopically light organic carbon was important during the onset of sapropel deposition.

On average, $\delta^{13}C_{org}$ values from MIS 5 sapropels in the eastern Mediterranean are 1‰ to 2‰ heavier than those in the Aegean Sea, which indicates a noticeably higher contribution of terrestrial organic carbon during sapropel deposition in the Aegean Sea relative to the eastern Mediterranean (Figure 9). Similarly, in the eastern Mediterranean sapropel S1, the $\delta^{13}C_{org}$ values are generally more enriched than those from the Aegean Sea.

4.1.2. C/S ratios

Sulfur and organic carbon relationships in modern and ancient sediments have been used to estimate bottom-water conditions at the time of deposition (e.g., Berner, 1984, 1989; Lin and Morse, 1991). The relationship between these elements can be a useful indicator for depositional environments (i.e. freshwater, normal marine, and anoxic/euxinic), since the biogeochemical cycle of sulfur is inseparable from that of carbon, and the relationship depends on the depositional environment (Berner, 1989). The sulfur in marine sediments is primarily contained in iron sulfide minerals (e.g., hydrotroilite, pyrite). Their amount in sediment is governed by the amount/reactivity of organic matter, the availability of dissolved sulfate, and the content/reactivity of iron minerals (Berner, 1984). In normal marine sediments there is a good correlation between organic carbon and pyrite sulfur with a constant C/S ratio of about 2.8 on a weight basis (Berner, 1984). According to Berner (1984), the constant C/S ratio in normal marine sediments is due to constant fractions of organic carbon and reduced sulfur being preserved in the sediments, with organic matter limiting the amount of iron

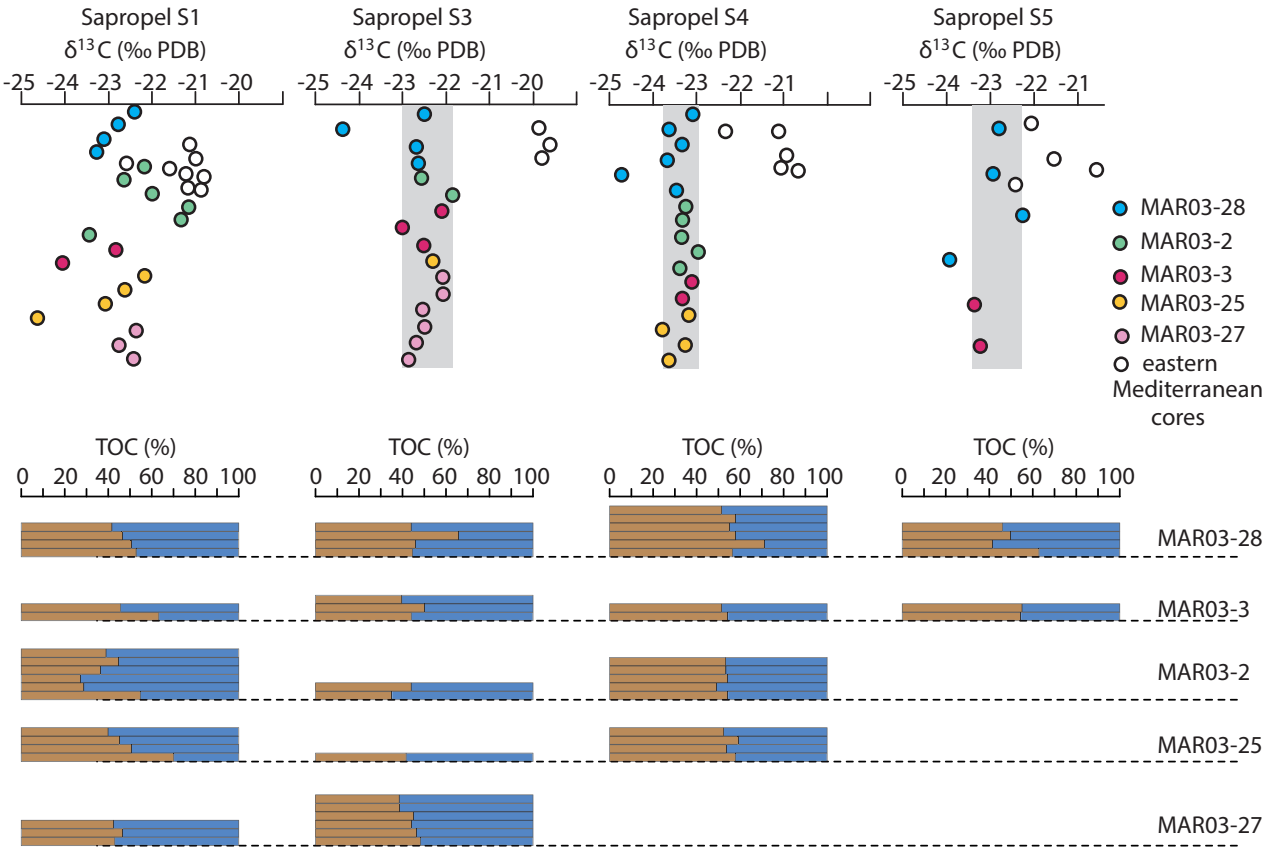

Figure 9. Values of $\delta^{13}C$ in total organic carbon, and terrestrial fractions calculated from the isotopic data, for sapropels S1, S3, S4, and S5. For comparison, carbon isotopic values from the eastern Mediterranean sediments (white circles) are also shown with end members specified in the text. F_{terr} = terrestrial fraction, determined from the linear mixing equation $\delta^{13}C = F_{terr} \times (-28‰) + (1 - F_{terr}) \times (-19‰)$ (data from M Paterne, unpublished eastern Mediterranean data; ten Haven et al., 1987; Sutherland et al., 1984). The lower bar graphs show terrestrial (brown) and marine (blue) fractions calculated for each data point in the sapropel.

sulfide formed. For freshwater sediments, the availability of sulfate ions limits the amount of iron sulfide formed, resulting in a much higher C/S ratio than in normal marine sediments (Berner and Raiswell, 1983, 1984). In euxinic sediments, given the excessive presence of H_2S and HS^- both in the water column and at the sediment–water interface, reactive iron determines the amount of iron sulfide formed irrespective of the amount of organic carbon present.

C/S plots in the cores show positive correlations ($0.63 < r < 0.86$), indicating that increased TOC was associated with higher sulfide precipitation. Such a relationship suggests that the main factor controlling the sulfur content in Aegean Sea sediments is the amount of organic matter rather than availability of dissolved sulfate or iron (Figure 10). The majority of the C/S ratios from the studied sapropels plot around the normal marine line, suggesting that these sapropels formed under normal marine conditions. In all five cores, C/S ratios from upper/top portions of S1 plot on the nonmarine line (Figure 10). Such low ratios might be explained by an increase in the freshwater/brackish water budget towards the end of sapropel formation, thereby limiting the availability of SO_4^{-2} and restricting the amount of S deposition as sedimentary sulfides. Several C/S ratios plotting well above the normal marine line and within the euxinic zone are observed in cores MAR03-28 and MAR03-27.

Samples with very high TOC values of 9%–12.5% in sapropel S5 (MAR03-28) plot below the normal marine line (Figure 9). With such high organic carbon contents, higher sulfur concentration would be expected. Less sulfide formation and/or sulfur uptake in the sediment might be ascribed to relatively higher fresh/brackish water input during the deposition of sapropel S5, perhaps elevated at the MAR03-28 site, which is at the northern end of the Aegean Sea nearest the outlet of the Strait of Dardanelles (Figure 1).

Fields defined by Stein (1986) for plots of sedimentation rate versus carbon content provide a preliminary assessment of both bottom-water oxygenation and sea-

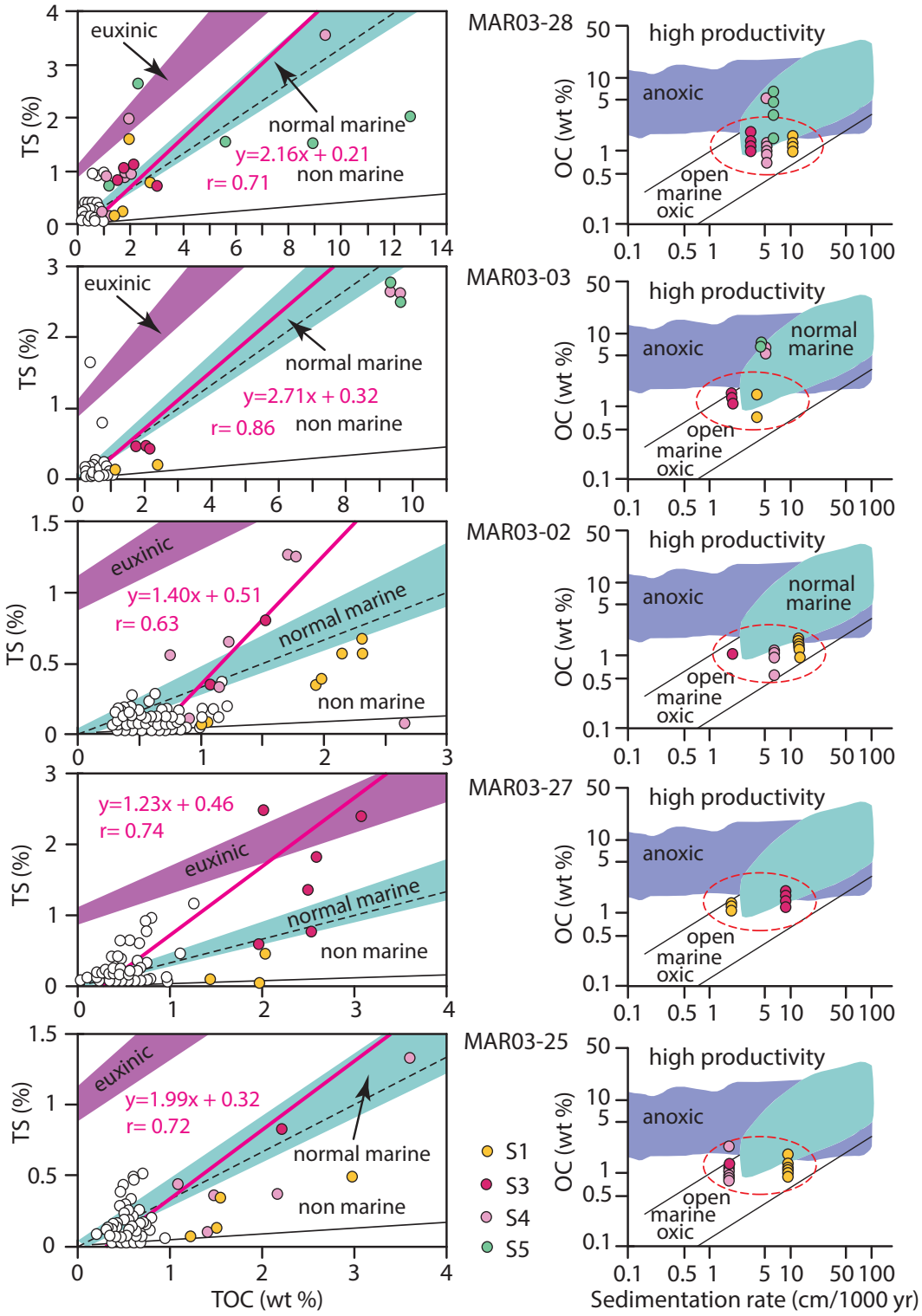

Figure 10. Left: Relationships between total organic carbon (TOC) and total sedimentary sulfur (TS), modified from Leventhal (1995); right: relationships between marine organic carbon (OC) and sedimentation rate (modified from Stein, 1986) showing the bottom-water conditions during the deposition of sapropels S1, S3, S4, and S5. Dashed line on left is C/S = 1:2.8 reference line (from Berner, 1984). White circles = data from nonsapropel sediments. Yellow, purple, pink, and green circles represent data from sapropels S1, S3, S4, and S5, respectively. Regression lines (red) are based on all data points. Anoxic, high-productivity and normal-marine fields are based on data from Recent to Miocene sediments with insignificant amounts of terrestrial organic carbon, deposited under oxic and anoxic sea-water conditions (Leventhal, 1995).

surface primary productivity (Figure 10). Such plots are only valid for the marine component of the organic carbon fraction (OC), since the terrestrial component has no bearing on sea-surface productivity. Plots of sedimentation rate versus OC for the Aegean Sea sapropel units show a clear clustering in the 'open marine oxic' field, except that samples with very high TOC values (S4 and S5 in cores MAR03-28 and MAR03-3) plot within or near the anoxic field (Figure 10). These same samples plot either along the normal marine line or below it.

4.1.3. $\delta^{34}S$ values

Core top $\delta^{34}S$ values range between +9‰ and +11‰ with maximum and minimum values of +14‰ and –0.8‰ in cores MAR03-28 and MAR03-27, respectively (Figure 8). These values are comparatively lighter than the Mediterranean seawater value of +20.6‰ reported by de Lange et al. (1990). The $\delta^{34}S$ signal difference of 10‰–20‰ between the Aegean core tops and Mediterranean seawater can be attributed to the following four factors: (i) the $\delta^{34}S$ values of sulfate diffusing into Aegean Sea sediments is probably lighter than that of seawater as a consequence of preferential diffusion of ^{32}S (Jorgensen, 1978; Chanton et al., 1987), (ii) part of the sulfur pool in the partly isolated Aegean Sea might originate from freshwater sulfate, (iii) isotope exchange reactions may have weakened the isotope signal (Fossing and Jørgensen, 1990), and (iv) coretop samples might have a mixture of sulfur with a primary seawater-sulfate signature and sulfur (as FeS) fixed during the first stages of early diagenetic sulfate reduction, which involves a large negative isotopic shift.

In MIS 5 sapropels, the $\delta^{34}S$ values range between –40‰ and –45‰, whereas in sapropel S1, the $\delta^{34}S$ values range between –30‰ and –35‰ in cores MAR03-27, MAR03-25, and MAR03-3 and –40‰ and –42‰ in cores MAR03-28 and MAR03-2 (Figure 8). These light values imply that fractionations of at least 60‰–65‰ occurred relative to Mediterranean seawater. To achieve fractionations of sulfur isotopes of this magnitude between sulfate and pyrite, sulfate reduction must have proceeded with a continuous and abundant supply of dissolved sulfate (open system) where exchange between near-surface pore waters and seawater readily occurred, followed by further $\delta^{34}S$ depletion in the sulfide pool by reoxidation and disproportionation processes in the sulfur cycle (Passier et al., 1999). Provided that benthic fauna were continuously present during sapropel accumulation (to account for widely developed bioturbation) so that bottom waters were never anoxic, the appropriate geochemical conditions likely occurred immediately below the sediment-water interface as a result of a large SO_4^{2-} supply via diffusion or advection relative to the SO_4^{2-} reduction rates, so that SO_4^{2-} was never depleted.

Across sapropels, the $\delta^{34}S$ values show similar values irrespective of the amount of TOC present (Figure 8). Even in sapropel S5 (12.5% TOC) the $\delta^{34}S$ fractionations are similar to those for sediments with TOC contents of ~2%, implying that all sulfate reduction occurred below the sediment–water interface. Significantly lighter $\delta^{34}S$ values in sapropel units (~40‰) as opposed to intervening nonsapropel layers (~2‰) suggest the presence of dysoxic bottom waters and near-surface pore waters to encourage thorough sulfate reduction, a suggestion that is supported by the dominance of *Chondrites* burrows in the sapropels (Löwemark et al., 2006). Moreover, maximum depletions across sapropels are even more negative than those observed in Holocene shelf muds from the southwestern Black Sea (e.g., about –32‰; Hiscott et al., 2007), probably because the Aegean Sea has a higher sulfate content due to its higher salinity.

4.2. Paleoproductivity

Sapropels are reported to form at times of elevated productivity in the surface waters (e.g., Rossignol-Strick et al., 1982; Calvert et al., 1992; Murat and Göt, 2000; Kouli et al., 2012). Estimates of the organic carbon that is exported from the photic zone into the deep sea, called the export paleoproductivity (PP), have been obtained using equations from two empirical studies. Eq. (1) is simplified from equations 1, 2, and 8 of Howell and Thunell (1992) and incorporates a preservation factor (pf), which those authors indicate to be 0.2%–0.5% in oxic marine environments, ~2.5% for the most poorly oxygenated sites in the Bannock Basin, and ~5% in the anoxic Black Sea.

$$PP_1 = \frac{OC*LSR*(dw - (1.025*\Phi))}{10*pf} \quad (1)$$

Eq. (2) is from Müller and Suess (1979).

$$PP_2 = \frac{OC*dg*(1-\Phi)}{0.003*LSR^{0.3}} \quad (2)$$

PP has units of g C m^{-2} $year^{-1}$ (g C = grams carbon). LSR is the linear sedimentation rate (cm ka^{-1}). Parameters fixed in the analysis presented here are d_w = the sediment wet density = 1.5 g cm^{-3}, d_g = the sediment grain density = 2.7 g cm^{-3}, and Φ = the fractional porosity = 0.72. In Eq. (1), PP_1 and pf are both unknowns (within realistic limits defined by other studies), so a unique solution is not possible. As input to both Eqs. (1) and (2), LSR is crudely captured by the age models for the five cores (Figure 11), but it is not known with sufficient temporal resolution to investigate what might be important differences between sapropel and nonsapropel sedimentation rates. This issue is explored in Section 4.

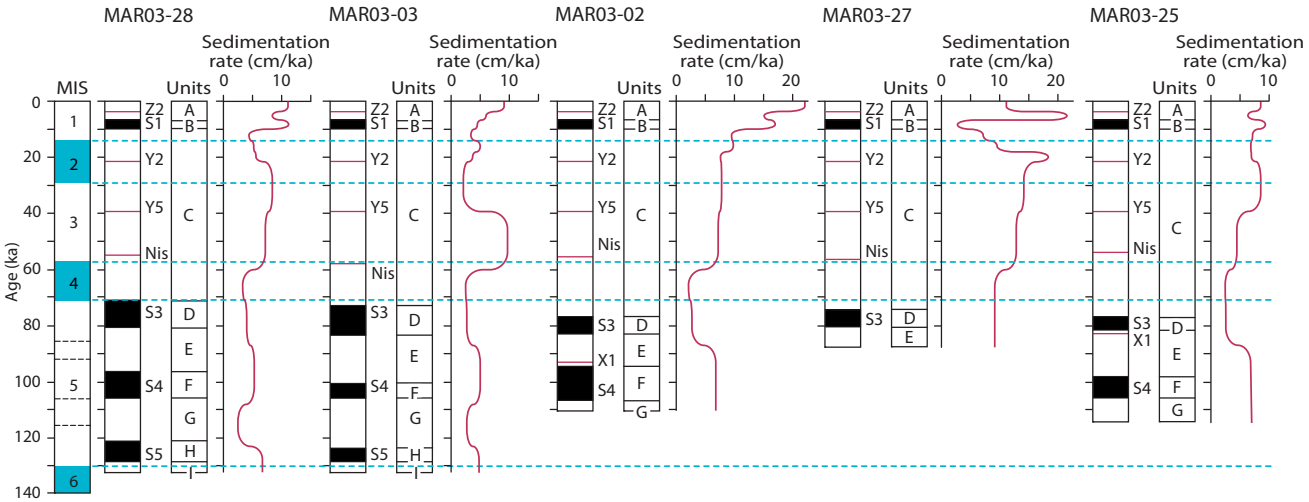

Figure 11. Age-converted plots showing the variations in sedimentation rates in lithostratigraphic units A through I in the Aegean Sea cores. Ash layers Z2, Y2, Y5, Nis, and X1 (red fills) are from Aksu et al. (2008). Sapropels are shown as black fills with S1, S3, S4, and S5 designations. Global oxygen isotopic stage boundaries from Lisiecki and Raymo (2005). Core locations are shown in Figure 1.

Eqs. (1) and (2) appear quite dissimilar but are actually equivalent under most open-marine conditions. This is because pf, as a decimal fraction, is a function of LSR alone in nonrestricted seas (regression coefficient R^2 = 0.98; Müller and Suess, 1979; their figure 5 and equation 5). Specifically:

$$pf = 0.00030\ LSR^{1.30} \quad (3)$$

Substituting Eq. (3) and fixed parameters into Eq. (1) gives:

$$PP_1 = \frac{254 * OC}{LSR^{0.3}} \quad (4)$$

Substituting fixed parameters into Eq. (2) gives an essentially identical equation:

$$PP_2 = \frac{252 * OC}{LSR^{0.3}} \quad (5)$$

The only difference in the approach of Howell and Thunell (1992) is their introduction of a preservation factor that can be varied independently of the LSR, whereas Müller and Suess (1979) ascribed preservation entirely to changes in sedimentation rate. Interestingly, Müller and Suess (1979) provided examples of pf as high as 18% in some Baltic Sea sediments. They noted, however, that in strongly stratified conditions or with significant inputs of terrestrial organic matter, the preservation factor deviates from Eq. (5). In the Black Sea, for example, the percentage of the surface organic-matter production preserved in sediments is 4–5 times higher than predicted by Eq. (5).

The amount of organic carbon preserved in sediments is primarily controlled by the sedimentation rate and the amount of primary production within the photic zone. Extracting estimates of primary paleoproductivity is highly dependent on an accurate knowledge of sedimentation rates. Even with known rates, Müller and Suess (1979) attached an uncertainty of 200% to calculated values. Because of the rather high uncertainty in results expected from Eqs. (1) and (2), other relatively small analytical uncertainties (e.g., in TOC and marine organic carbon (OC_{mar}) content) are not tracked through the discussion. The reader should therefore view final conclusions of this paper as somewhat qualitative, although based on underlying hard analytical results from the 5 piston cores.

The sedimentation rate at a core location is controlled by several factors such as distance to source (e.g., river mouth), water depth, and sea bed morphology. Higher sedimentation rates will increase the burial rate of the organic matter, thus decreasing the time of exposure to oxic degradation. High sedimentation rates will also dilute organic carbon concentrations so that the TOC content of a sampled interval (e.g., sapropel) may not represent the actual organic carbon flux to the sea floor. The calculation of paleoproductivity values thus depends on how accurately the sedimentation rate and the organic carbon flux during a particular time interval can be specified. Sedimentation rates throughout the Aegean Sea exhibit a wide range from 2.9 cm ka^{-1} to as high as 58.5 cm ka^{-1} (Aksu et al., 1995; Roussakis et al., 2004; Casford, et al., 2007) with an average range of 10–13 cm ka^{-1}. Age tie-points in the Aegean Sea cores provide the sedimentation rates used in this paper (Figure 11), but short-term rates from the base

to the top of individual sapropel units are not available, introducing some uncertainty into the paleoproductivity analysis. Sedimentation rates higher than 20 cm ka^{-1} have been reported for sapropel S1; however, most researchers report a range between 9 cm ka^{-1} and 14 cm ka^{-1} with an average sedimentation rate of 12 cm ka^{-1} (Aksu et al., 1995a, 1995b; Casford et al., 2002; Roussakis et al., 2004; Gogou et al., 2007). The sedimentation rates for MIS 5 sapropels range between 2.9 cm ka^{-1} and 9.1 cm ka^{-1} with an average range of 4–6 cm ka^{-1}. These are all less than the rate of 25.2 cm ka^{-1} that was reported for sapropel S5 in core LC21 northeast of Crete (Casford et al., 2002), far from the core locations considered in this paper.

Müller and Suess (1979) did not include sediments accumulating under permanently anoxic bottom water in their empirical regression analysis. Because the bottom-water conditions during accumulation of sapropels S1, S3, S4, and S5 in the Aegean Sea were never anoxic (İşler, 2012), it is valid to use Eq. (2) to infer past sea water productivity variations as downcore PP_2 profiles. Both Eqs. (1) and (2) were developed for areas with negligible delivery of terrigenous organic matter to the sea floor, which is not the case for the Aegean Sea because of its semienclosed geography and significant riverine input through several rivers and the Dardanelles Strait. The $\delta^{13}C_{org}$ values show equally important organic matter contributions from both marine and terrestrial sources (Figures 9 and 12). Only the marine fraction (i.e. OC) is relevant to paleoproductivity calculations, and it is this fraction that is used to generate downcore profiles for the five Aegean Sea cores (Figure 13); downcore preservation factors consistent with Eq. (1) and these paleoproductivity values are derived either from Eq. (3) or by setting $PP_1 = PP_2$ and solving Eq. (1) for pf. Although quantitative paleoproductivity calculations might be viewed with skepticism due to their high sensitivity to sedimentation rates, they do have the potential to provide valuable insight into past primary productivity fluctuations at the sea surface.

Except near the top of core MAR03-02 and the central part of core MAR03-27, the calculated nonsapropel preservation factors are ≤1% and mostly <0.5%. Many of these values are within the range of 0.2%–0.5% postulated for oxic marine environments by Howell and Thunell (1992).

4.3. Assessment of the paleoproductivity estimates for sapropel units

Paleoproductivity values calculated with Eq. (2) (Müller and Suess, 1979) are mostly <300 g C m^{-2} $year^{-1}$, except in sapropels S4 (core MAR03-28) and S5 (cores MAR03-03 and MAR03-28). S5, in particular, has calculated paleoproductivity values as high as ~1000 g C m^{-2} $year^{-1}$. These latter values suggest that the surface productivity was at least 30 times higher than present-day surface productivity in the Aegean Sea (30 g C m^{-2} $year^{-1}$), exceeding (in the case of S5) the productivity in modern upwelling regions where values reach 500 g C m^{-2} $year^{-1}$. Actualism speaks strongly against such high paleoproductivities. Instead, it is proposed that preservation levels, at least during the accumulation of S4 and S5, must have been higher than predicted by Eq. (3), similar to the situation in the Black Sea (but to a lesser degree) where preservation factors are ~4–5 times those predicted by Eq. (3) (Müller and Suess, 1979). As explained by the latter authors, extraordinary preservation of the export production from surface waters can result from bottom-water oxygen depletion (or absence). Water-column stratification and poor bottom-water ventilation (hence low O_2 levels) in the semienclosed Aegean Sea during times of surface freshening would have decreased the amount of primary production needed to account for the observed OC_{mar} abundances. *Chondrites* burrows in all Aegean Sea sapropels are inconsistent with anoxia, but instead indicate low oxygen levels in bottom waters and the uppermost sediments. For this reason, it is more likely that the appropriate preservation factor to use in Eq. (1) is a few times higher than predicted by Eq. (3), but not as high as 5.

The presence in the sediments of significant terrigenous organic carbon, particularly in sapropels, might have created an additional boost to the preservation potential of the comingled marine OC, leading to an additional overestimation of required primary paleoproductivity levels. The $\delta^{13}C_{org}$ values show that both marine and terrestrial organic matter contributed equally to MIS 5 sapropels S3, S4, and S5. Across sapropel S1, upward carbon-isotopic enrichment suggests a progressively diminishing terrigenous input toward the end of sapropel deposition. The $\delta^{13}C_{org}$ values in the Aegean Sea sapropels are 1‰–2‰ more depleted than their Mediterranean Sea counterparts, signifying a stronger terrestrial contribution to the pool of organic matter, thus likely an enhanced riverine input during the deposition of the MIS 5 sapropels S3, S4, and S5. The paleoproductivity estimates of Eq. (2) (Figure 13) ignored the terrigenous component of the TOC in the Aegean Sea sapropels. Preservation of the terrigenous component is considerably higher in sapropels S1–S5 than in background sediments. This might indicate higher fluxes from coastal rivers at those times, but it is also possible that higher levels of OC_{mar} accumulation, moderate bottom-water stagnation, and elevated preservation factors facilitated an enhanced level of preservation for terrigenous organic carbon, even if its delivery into the Aegean Sea was approximately constant through time. The extra carbon load from terrigenous input would intensify water column stratification and impede advection of oxygenated surface waters, further

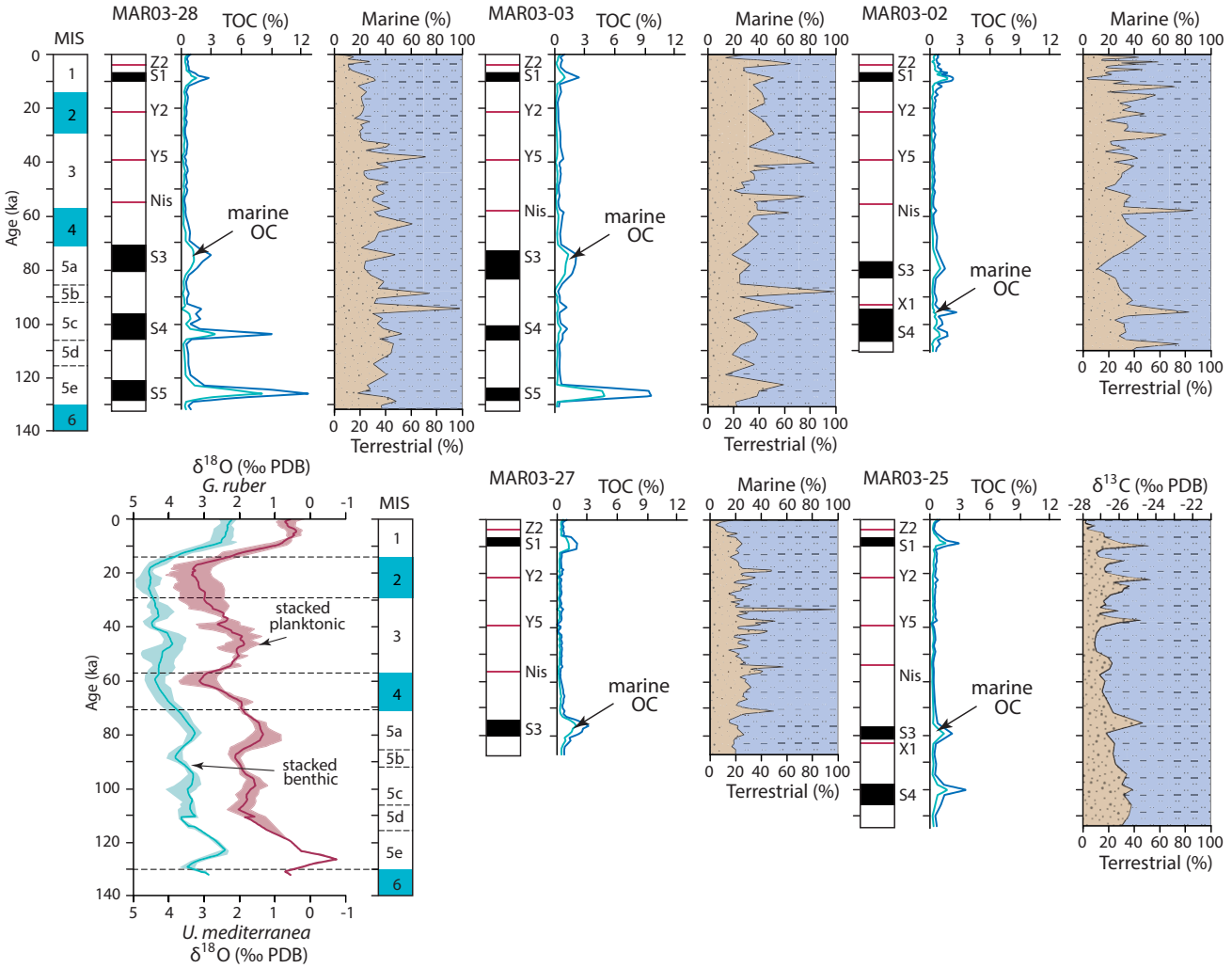

Figure 12. Downcore plots showing the total organic carbon (TOC) contents and variations in the proportions and percentages of marine (blue, OC) and terrestrial (brown) fractions of the total organic carbon in the Aegean Sea cores. MIS = marine isotopic stages. Black fills = sapropels, red fills = volcanic ash layers (from Aksu et al., 2008). Stacked oxygen isotope curves are from Figure 6. Core locations are shown in Figure 1.

promoting bottom-water stagnation and thus improved preservation (e.g., dysoxia). In this scenario, the marine flux and structure of the water column could have provided the trigger for sapropel onset, and the terrestrial flux might then have amplified these conditions so as to ensure strong organic-matter preservation.

Finally, there is one additional factor that might have contributed to the locally high OC_{mar} contents of S3–S5: the interpreted presence of a deep chlorophyll maximum (DCM) layer (İşler et al., 2016). A DCM layer will develop if the nutricline/chemocline rises toward shallower waters because of a decreased density contrast between the surface and intermediate waters. Shoaling of the pycnocline above the thermocline and into the lower portions of the photic zone could contribute greatly to the export production by adding a new contribution of organic detritus from biological activity at the base of the photic zone, even if the contemporary productivity of the surface waters was not exceptional. In contrast, the relatively high PP values calculated for sapropel S1 (Figure 13) are needed to provide sufficient carbon flux to the sea floor because a DCM layer was absent at that time, as demonstrated by the disappearance of *N. pachyderma* (d) immediately below the sapropel (Rohling and Gieskes, 1989; Rohling et al., 1993).

4.4. Depositional model for Aegean Sea sapropels

A plausible, qualitative depositional model is illustrated using data from core MAR03-28 (Figure 14). Through the intervals of sapropel accumulation, pf values have been multiplied by a factor of 4 to qualitatively illustrate

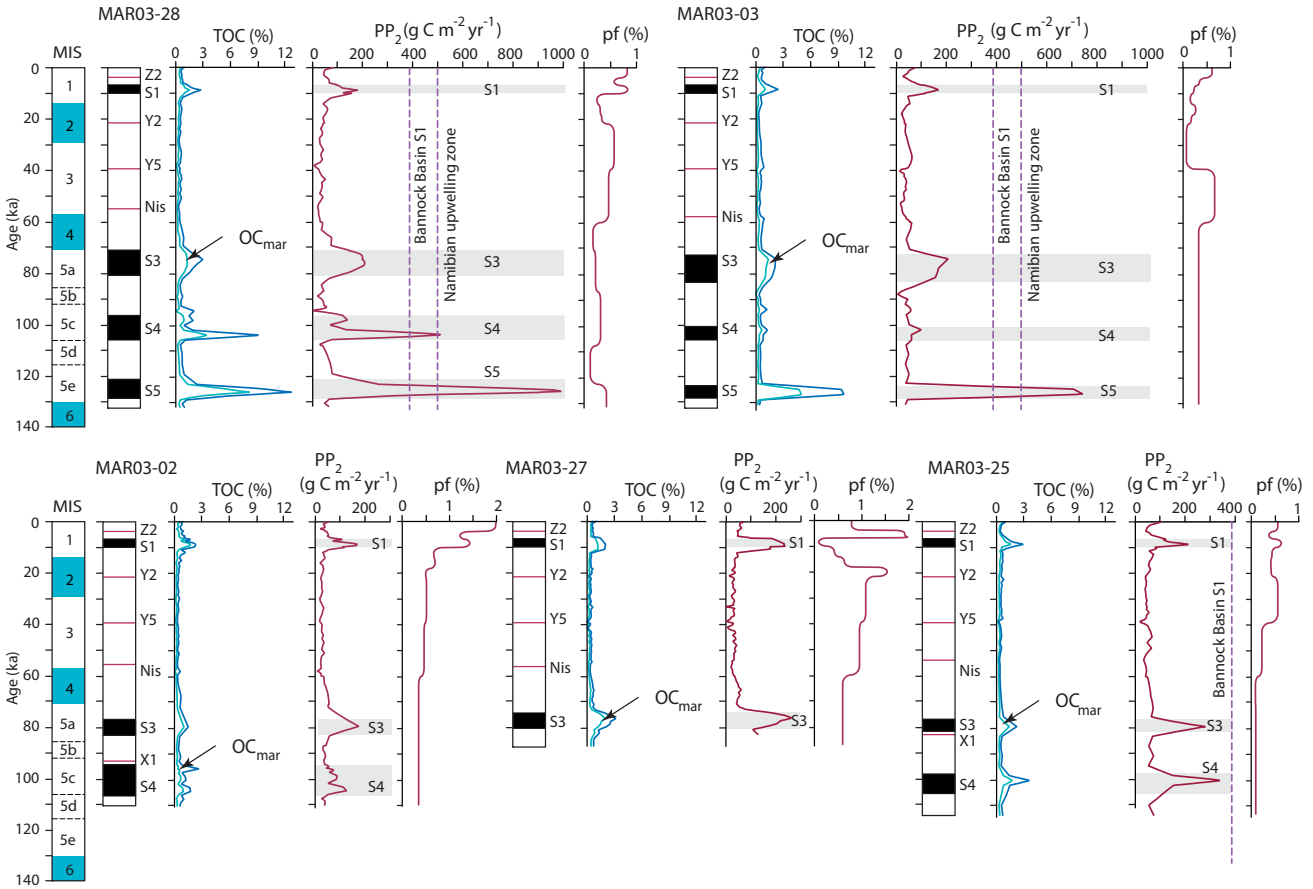

Figure 13. Downcore plots showing the total organic carbon (TOC) and marine organic carbon (OC_{mar}) contents, primary productivity (PP_2) values calculated using the equations of Müller and Suess (1979), and preservation factors consistent with $PP_1 = PP_2$ in the Aegean Sea cores (explained in the text). Vertical dashed lines in selected PP_2 plots mark the maximum values reported by Howell and Thunell (1992) for the Bannock Basin (393 g C m^{-2} $year^{-1}$ for sapropel S1) and the Namibian upwelling zone (500 g C m^{-2} $year^{-1}$). MIS = marine isotopic stages. Black fills = sapropels, red fills = volcanic ash layers (from Aksu et al., 2008). Core locations are shown in Figure 1.

the effects of enhanced preservation levels caused by a combination of water-column stratification, buffering of low oxygen levels by the load of terrestrial organic carbon, and contribution to the carbon flux from a deep chlorophyll maximum layer. With higher pf values than those typical of open-ocean settings, Eq. (1) gives primary paleoproductivity estimates significantly lower in sapropel units than those in Figure 13 that were based on Eq. (2). The degree to which pf should be incremented to reflect past conditions is not known with any certainty, except that for sapropel S1 the extent of enhanced preservation might reasonably be lower than for S3–S5 because of the lack of a deep chlorophyll maximum in this youngest sapropel. However, Figure 14 provides some useful constraints on the paleoceanographic conditions during sapropel accumulation. In particular, higher pf values succeed in reducing the calculated PP values to levels consistent with modern zones of organic matter accumulation like the Bannock Basin and zones of upwelling. Nevertheless, some increase in the level of primary productivity above the modern 30 g C m^{-2} $year^{-1}$ is unavoidable to maintain realistic pf values and to explain the triggering of sapropel events. It is a reasonable conclusion that a combination of enhanced primary productivity, some degree of water-column stratification, and a good supply of terrigenous organic carbon and nutrients from continental runoff all contributed to sapropel development. Refinement of this model will require more tightly constrained sedimentation rates from older sapropels, which is a difficult proposition because these units are too old to be dated by radiocarbon techniques, and age tie-points of any kind do not lie precisely at sapropel boundaries, a requirement if there is a strong facies control on accumulation rates.

C/S plots suggest that sapropels S1, S3, S4, and S5 were deposited under normal marine conditions with possible establishment of near-euxinic bottom-water conditions. Highly depleted and relatively uniform $\delta^{34}S$ values together with the absence of fully euxinic conditions during

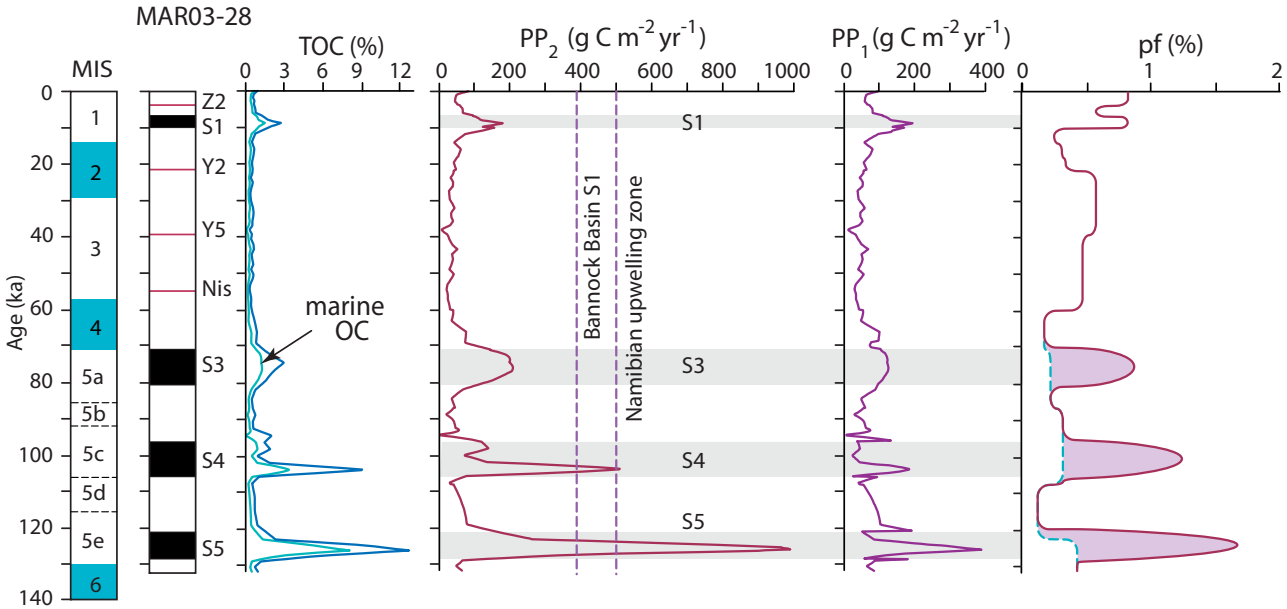

Figure 14. Hypothetical evaluation of the implications of elevated preservation factors (pf) during accumulation of sapropels S3, S4, and S5 in core MAR03-28, for reasons explained in the text. For these three sapropels, the pf values of Figure 13 were increased by a factor of 4 (shaded peaks), reflecting stronger ocean stratification and poorer bottom-water ventilation, and then primary productivity values in the same intervals were recalculated using Eq. (1) (giving the PP_1 profile), leading to a reduction in the extreme values shown in the PP_2 profile, for which pf values were derived from Eq. (3).

sapropel accumulation suggest that sulfate reduction took place consistently below the sediment–water interface and not in the water column.

Acknowledgments

We thank Dr Doğan Yaşar for his continued support and the officers and crew of the *RV Koca Piri Reis* of the Institute of Marine Sciences and Technology, Dokuz Eylül University, for their assistance in data acquisition. We acknowledge research and ship-time funds from the Natural Sciences and Engineering Research Council of Canada (NSERC) to Aksu and Hiscott; travel funds from the Dean of Science, Memorial University of Newfoundland; and a special grant from the VP Research, Memorial University of Newfoundland. We thank Alison Pye for her assistance in the stable isotopic and elemental analyses. We thank the Manuscript Editor Dr Alessandro Incarbona for his valuable comments.

References

Abu-Zied RH, Rohling EJ, Jorissen FJ, Fontanier C, Casford JSL, Cooke S (2008). Benthic foraminiferal response to changes in bottom-water oxygenation and organic carbon flux in the eastern Mediterranean during LGM to Recent times. Mar Micropaleontol 67: 46–68.

Aksu AE, Jenner G, Hiscott RN, İşler EB (2008). Occurrence, stratigraphy and geochemistry of Late Quaternary tephra layers in the Aegean Sea and the Marmara Sea. Mar Geol 252: 174–192.

Aksu AE, Yaşar D, Mudie PJ (1995a). Paleoclimatic and paleoceanographic conditions leading to development of sapropel layer S1 in the Aegean Sea. Palaeogeogr Palaeocl 116: 71–101.

Aksu AE, Yaşar D, Mudie PJ, Gillespie H (1995b). Late glacial–Holocene paleoclimatic and paleoceanographic evolution of the Aegean Sea: micropaleontolological and stable isotopic evidence. Mar Micropaleontol 25: 1–28.

Berner RA (1984). Sedimentary pyrite formation: an update. Geochim Cosmochim Ac 48: 605–615.

Berner RA (1989). Biogeochemical cycles of carbon and sulfur and their effect on atmospheric oxygen over Phanerozoic time. Global Planet Change 75: 97–122.

Berner RA, Raiswell R (1983). Burial of organic carbon and pyrite sulfur in sediments over Phanerozoic time: a new theory. Geochim Cosmochim Ac 47: 55–62.

Berner RA, Raiswell R (1984). C/S method for distinguishing freshwater from marine sedimentary rocks. Geology 12: 65–68.

Calvert SE (1983). Geochemistry of Pleistocene sapropels and associated sediments from the eastern Mediterranean. Oceanol Acta 6: 255–267.

Calvert SE, Nielsen B, Fontugne MR (1992). Evidence from nitrogen isotope ratios for enhanced productivity during formation of eastern Mediterranean sapropels. Nature 359: 223–225.

Casford JSL, Abu Zied R, Rohling EJ, Cooke S, Fontanier C, Leng M, Millard A, Thomson J (2007). A stratigraphically controlled multiproxy chronostratigraphy for the eastern Mediterranean. Paleoceanography 22: PA4215.

Casford JSL, Rohling EJ, Abu Zied RH, Cooke S, Fontanier C, Leng M, Lykousis V (2002). Circulation changes and nutrient concentrations in the late Quaternary Aegean Sea: a nonsteady state concept for sapropel formation. Paleoceanography 17: 1024.

Chanton JP, Martens CS, Goldhaber MB (1987). Biogeochemical cycling in an organic-rich coastal marine basin. 7. Sulfur mass balance, oxygen uptake and sulfide retention. Geochim Cosmochim Ac 51: 1187–1199.

Cita MB, Grignani D (1982). Nature and origin of Late Neogene Mediterranean sapropels. In: Schlanger SO, Cita MB, editors. Nature and Origin of Cretaceous Carbon-Rich Facies. London, UK: Academic Press, pp. 165–196.

Cita MB, Podenzani M (1980). Destructive effects of oxygen starvation and ash fall on benthic life: a pilot study. Quataternary Res 13: 230–241.

Cramp A, O'Sullivan G (1999). Neogene sapropels in the Mediterranean: a review. Mar Geol 153: 11–28.

Deines P (1980). The isotopic composition of reduced organic carbon. In: Fritz P, Fontes JC, editors. Handbook of Environmental Isotope Geochemistry: The Terrestrial Environment, A. Amsterdam, the Netherlands: Elsevier, pp. 329–406.

de Lange GJ, Middelburg JJ, van der Weijden CH, Catalano G, Luther GW 3rd, Hydes DJ, Woittiez JRW, Klinkhammer GP (1990). Composition of anoxic hypersaline brines in the Tyro and Bannock Basin, eastern Mediterranean. Mar Chem 31: 63–88.

Demaison GJ, Moore GT (1980). Anoxic environments and oil source bed genesis. AAPG Bulletin 64: 1179–1209.

de Rijk S, Hayes A, Rohling EJ (1999). Eastern Mediterranean sapropel S1 interruption: an expression of the onset of paleoceanographic conditions leading to development of climatic deterioration around 7 ka BP. Mar Geol 153: 337–343.

Emeis KC, Sakamoto T, Wehausen R, Brumsack HJ (2000). The sapropel record of the eastern Mediterranean Sea - results of Ocean Drilling Program Leg 160. Palaeogeogr Palaeoecol 158: 371–395.

Emeis KC, Schulz H, Struck U, Rossignol-Strick M, Erlenkeuser H, Howell MW, Kroon D, Mackensen A, Ishizuka S, Oba T et al. (2003). Eastern Mediterranean surface water temperatures and $\delta^{18}O$ composition during deposition of sapropels in the late Quaternary. Paleoceanography 18: 1005.

Fontugne MR, Calvert SE (1992). Late Pleistocene variability of the carbon isotopic composition of organic matter in the eastern Mediterranean: monitor of changes in carbon sources and atmospheric CO_2 concentrations. Paleoceanography 7: 1–20.

Fossing H, Jørgensen BB (1990). Oxidation and reduction of radiolabeled inorganic sulfur compounds in an estuarine sediment, Kysing Fjord, Denmark. Geochim Cosmochim Ac 54: 2731–2742.

Gogou A, Bouloubassi I, Lykousis V, Arnaboldi M, Gaitani P, Meyers PA (2007). Organic geochemical evidence of Late Glacial-Holocene climate instability in the North Aegean Sea. Palaeogeogr Palaeoecol 256: 1–20.

Grant KM, Rohling EJ, Bar-Matthews M, Ayalon A, Medina-Elizalde M, Bronk Ramsey C, Satow C, Roberts AP (2012). Rapid coupling between ice volume and polar temperature over the past 150,000 years. Nature 491: 744–747.

Grelaud M, Marino G, Ziveri P, Rohling EJ (2012). Abrupt shoaling of the nutricline in response to massive freshwater flooding at the onset of the last interglacial sapropel event. Paleoceanography 27: PA3208.

Herman Y (1981). Paleoclimatic and paleohydrologic record of Mediterranean deep-sea cores based on pteropods, planktonic and benthic foraminifera. Rev Esp Micropaleontol 8: 171–200.

Hiscott RN, Aksu AE, Mudie PJ, Marret F, Abrajano T, Kaminski MA, Evans J, Çakıroğlu AI, Yaşar D (2007). Gradual drowning of the southwestern Black Sea shelf: evidence for a progressive rather than abrupt Holocene reconnection with the eastern Mediterranean Sea through the Marmara Sea Gateway. Quatern Int 167–168: 19–34.

Howell MW, Thunell RC (1992). Organic carbon accumulation in Bannock Basin: evaluating the role of productivity in the formation of eastern Mediterranean sapropels. Mar Geol 103: 461–471.

İşler EB, Hiscott RN, Aksu AE (2016). Late Quaternary chronostratigraphy of the Aegean Sea sediments with special reference to the ages of sapropels S1–S5. Turkish J Earth Sci 25: 1–18.

Jørgensen BB (1978). A comparison of methods for the quantification of bacterial sulfate reduction in coastal marine sediments. I: Measurements with radiotracer techniques. Geomicrobiol J 1: 11–27.

Kotthoff U, Pross J, Muller UC, Peyrono O, Schmiedl G, Schulz H, Bordon A (2008). Climate dynamics in the borderlands of the Aegean Sea during formation of sapropel S1 deduced from a marine pollen record. Quaternary Sci Rev 27: 832–845.

Kouli K, Gogou A, Bouloubassi I, Triantaphyllou MV, Ioakim C, Katsouras G, Roussakis G, Lykousis V (2012). Late postglacial paleoenvironmental change in the northeastern Mediterranean region: combined palynological and molecular biomarker evidence. Quatern Int 261: 118–127.

Leventhal JS (1995). Carbon-sulfur plots to show diagenetic and epigenetic sulfidation in sediments. Geochim Cosmochim Ac 59: 1207–1211.

Lin S, Morse JW (1991). Sulfate reduction and iron sulfide mineral formation in Gulf of Mexico anoxic sediments. Am J Sci 291: 55–89.

Lisiecki LE, Raymo ME (2005). A Pliocene-Pleistocene stack of 57 globally distributed benthic $\delta^{18}O$ records. Paleoceanography 20: PA1003.

Löwemark L, Lin Y, Chen HF, Yang TN, Beier C, Werner F, Lee CY, Song SR, Kao SJ (2006). Sapropel burn-down and ichnological response to late Quaternary sapropel formation in two ~400 ky records from the eastern Mediterranean Sea. Palaeogeogr Palaeoecol 239: 406–425.

Lykousis V (2002). Circulation changes and nutrient concentrations in the late Quaternary Aegean Sea: a non-steady state concept for sapropel formation. Paleoceanography 17: 1024–1034.

McCorkle DC, Keigwin LD, Corliss BH, Emerson SR (1990). The influence of microhabitats on the carbon isotopic composition of deep-sea benthic foraminifera. Paleoceanography 5: 161–185.

Melki T, Kallel N, Fontugne M (2010). The nature of transitions from dry to wet condition during sapropel events in the Eastern Mediterranean Sea. Palaeogeogr Palaeoecol 291: 267–285.

Müller PJ, Suess E (1979). Productivity, sedimentation rate, and sedimentary organic matter in the oceans I. Organic carbon preservation. Deep Sea Res 26A: 1347–1362.

Mullineaux LS, Lohmann GP (1981). Late Quaternary stagnations and recirculation of the eastern Mediterranean: changes in the deep water recorded by fossil benthic foraminifera. J Foramin Res 11: 20–39.

Murat A, Göt H (2000). Organic carbon variations of the eastern Mediterranean Holocene sapropel: a key for understanding formation processes. Palaeogeogr Palaeoecol 158: 241–257.

Narcisi B, Vezzoli L (1999). Quaternary stratigraphy of distal tephra layers in the Mediterranean an overview. Global Planet Change 21: 31–50.

Passier HF, Bottcher ME, de Lange GJ (1999). Sulphur enrichment in organic matter of eastern Mediterranean sapropels: a study of sulphur isotope partitioning aquatic. Geochemistry 5: 99–118.

Pedersen TF, Calvert SE (1990). Anoxia versus productivity: what controls the formation of organic-carbon-rich sediments and sedimentary rocks? AAPG Bulletin 74: 454–466.

Roether W, Manca BB, Klein B, Bregant D, Georgopoulos D, Beitzel V, Kovacevic V, Luchetta A (1996). Recent changes in eastern Mediterranean deep water. Science 271: 333–335.

Rohling EJ (1994). Review and new aspects concerning the formation of eastern Mediterranean sapropels. Mar Geol 122: 1–28.

Rohling EJ, Gieskes WWC (1989). Late Quaternary changes in Mediterranean intermediate water density and formation. Micropaleontology 3: 147–173.

Rohling EJ, Jorissen FJ, Vergnaud-Grazzini C, Zachariasse WJ (1993). Northern Levantine and Adriatic Quaternary planktic foraminifera: reconstruction of paleoenvironmental gradients. Mar Micropaleontol 21: 191–218.

Rohling EJ, Sprovieri M, Cane T, Casford JSL, Cooke S, Bouloubassi I, Emeis KC, Schiebel R, Rogerson M, Hayes A et al. (2004). Reconstructing past planktic foraminiferal habitats using stable isotope data: a case history for Mediterranean sapropel S5. Mar Micropaleontol 50: 89–123.

Ross CR, Kennett JP (1984). Late Quaternary paleoceanography as recorded by benthonic foraminifera in Strait of Sicily sediment sequences. Mar Micropaleontol 8: 315–336.

Rossignol-Strick M (1985). Mediterranean Quaternary sapropels, an immediate response of the African monsoon to variation of insolation. Palaeogeogr Palaeoecol 49: 237–263.

Rossignol-Strick M, Nesteroff W, Olive P, Vergnaud-Grazzini C (1982). After the deluge: Mediterranean stagnation and sapropel formation. Nature 295: 105–110.

Roussakis G, Karageorgis AP, Conispoliatis N, Lykousis V (2004). Last glacial-Holocene sediment sequences in N. Aegean basins: structure, accumulation rates and clay mineral distribution. Geo-Mar Lett 24: 97–111.

Satow C, Tomlinson EL, Grant KM, Albert PG, Smith VC, Manning CJ, Ottolini L, Wulf S, Rohling EJ, Lowe JJ et al. (2015). A new contribution to the Late Quaternary tephrostratigraphy of the Mediterranean: Aegean Sea core LC21. Quat Sci Rev 117: 96–112.

Stefanelli S, Capotondi L, Ciaranfi N (2005). Foraminiferal record and environmental changes during the deposition of the Early-Middle Pleistocene sapropels in southern Italy. Palaeogeog Palaeoecol 216: 27–52.

Stein R (1986). Organic carbon and sedimentation rate—further evidence for anoxic deep water conditions in the Cenomanian/Turonian Atlantic Ocean. Mar Geol 72: 199–209.

Strohle K, Krom MD (1997). Evidence for the evolution of an oxygen minimum layer at the beginning of S-1 sapropel deposition in the eastern Mediterranean. Mar Geol 140: 231–236.

Struck U, Emeis KC, Voss M, Krom MD, Rau GH (2001). Biological productivity during sapropel S5 formation in the Eastern Mediterranean Sea: evidence from stable isotopes of nitrogen and carbon. Geochim Cosmochim Ac 65: 3249–3266.

van der Meer MTJ, Baas M, Rijpstra WIC, Marino G, Rohling EJ, Damsté JSS, Schouten S (2007). Hydrogen isotopic compositions of long-chain alkenones record freshwater flooding of the Eastern Mediterranean at the onset of sapropel deposition. Earth Planet Sc Lett 262: 594–600.

Velaoras D, Lascaratos A (2005). Deep water mass characteristics and inter-annual variability in the north and central Aegean Sea. J Marine Syst 53: 59–85.

Zervakis V, Georgopoulos D, Drakopoulos PG (2000). The role of the North Aegean in triggering the recent Eastern Mediterranean climatic changes. J Geophys Res 105: 26103–26116.

Zervakis V, Georgopoulos D, Karageorgis AG, Theocharis A (2004). On the response of the Aegean Sea to climatic variability: a review. Int J Climatol 24: 1845–1858.

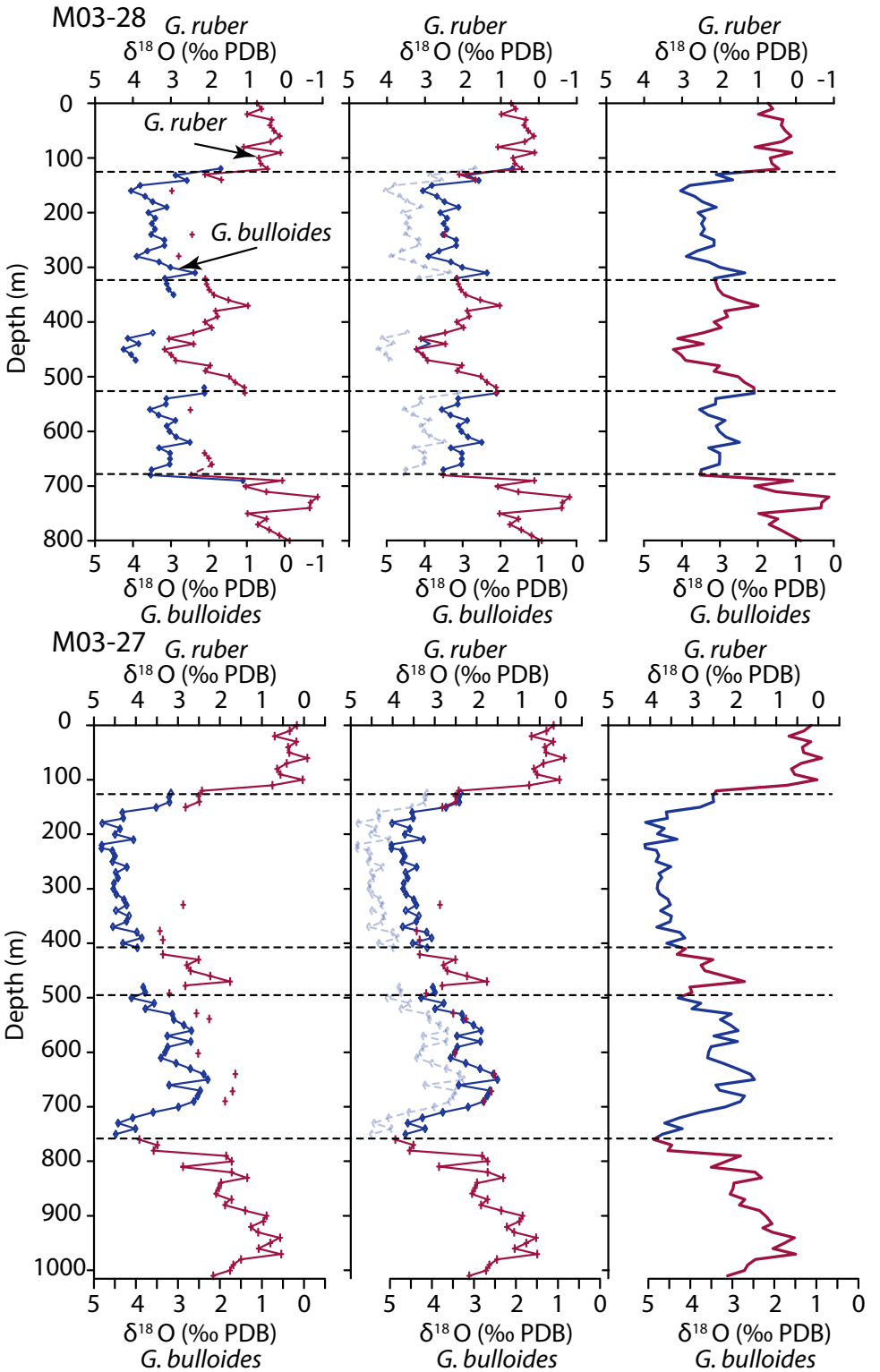

Appendix 1. Details of the raw oxygen isotopic data in cores MAR03-27 and MAR03-28, showing the construction of the pseudocomposite plot. Red and blue symbols and lines are the $\delta^{18}O$ values in planktonic foraminifera *G. ruber* and *G. bulloides*, respectively. Note that there are two scales in each graph. The pseudocomposite plot (column on far right) is carried forward into figures that require the oxygen isotopic records of cores MAR03-27 and MAR03-28.

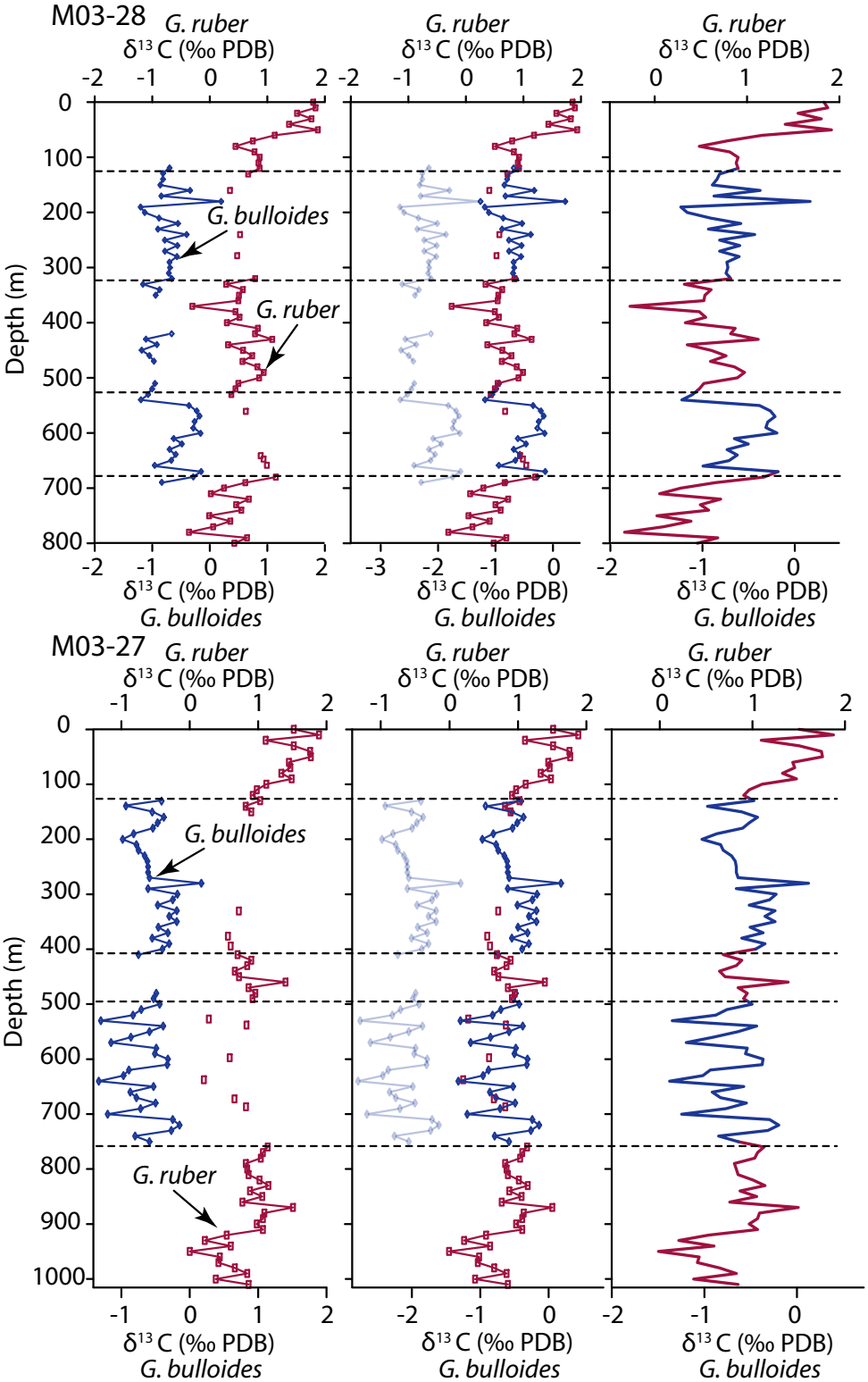

Appendix 2. Details of the raw carbon isotopic data in cores MAR03-27 and MAR03-28, showing the construction of the pseudocomposite plot. Red and blue symbols and lines are the $\delta^{13}C$ values in planktonic foraminifera *G. ruber* and *G. bulloides*, respectively. Note that there are two scales in each graph. The pseudocomposite plot (column on far right) is carried forward into figures that require the carbon isotopic records of cores MAR03-27 and MAR03-28.